# Discovery of (2S,3R)-N-[2-(Pyridin-3-ylmethyl)-1-azabicyclo[2.2.2]oct-3-yl]benzo[b]furan-2-carboxamide (TC-5619), a Selective α7 Nicotinic Acetylcholine Receptor Agonist, for the Treatment of Cognitive Disorders

Anatoly A. Mazurov,* David C. Kombo, Terry A. Hauser, Lan Miao, Gary Dull, John F. Genus, Nikolai B. Fedorov, Lisa Benson, Serguei Sidach, Yunde Xiao, Philip S. Hammond, John W. James, Craig H. Miller, and Daniel Yohannes

Targacept, Inc., Winston-Salem, North Carolina 27101-4165, United States

Ⓢ *Supporting Information*

ABSTRACT: (2S,3R)-N-[2-(Pyridin-3-ylmethyl)-1-azabicyclo[2.2.2]oct-3-yl]benzo[b]-furan-2-carboxamide (**7a**, TC-5619), a novel selective agonist of the α7 neuronal nicotinic acetylcholine receptor, has been identified as a promising drug candidate for the treatment of cognitive impairment associated with neurological disorders. **7a** demonstrated more than a thousand-fold separation between the affinities for the α7 and α4β2 receptor subtypes and had no detectable effects on muscle or ganglionic nicotinic receptor subtypes, indicating a marked selectivity for the central nervous system over the peripheral nervous system. Results obtained from homology modeling and docking explain the observed selectivity. **7a** had positive effects across cognitive, positive, and negative symptoms of schizophrenia in animal models and was additive or synergistic with the antipsychotic clozapine. Compound **7a**, as an augmentation therapy to the standard treatment with antipsychotics, demonstrated encouraging results on measures of negative symptoms and cognitive dysfunction in schizophrenia and was well tolerated in a phase II clinical proof of concept trial in patients with schizophrenia.
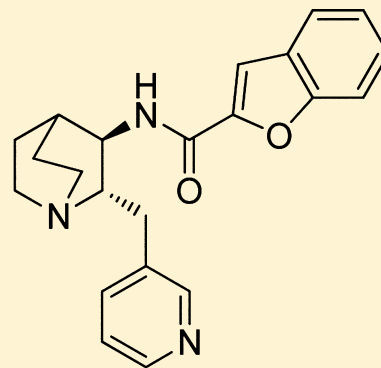
■ INTRODUCTION

Neuronal nicotinic acetylcholine receptors (nAChR) are pentameric ligand-gated ion channels of broad distribution and structural heterogeneity. Such diversity in both function and distribution indicates involvement in a variety of neuronal processes and has generated great interest in these acetylcholine receptors as targets for therapeutic intervention in a number of pathological conditions and diseases.[1] The α7 subtype (a homopentamer consisting of five α7 subunits) has been extensively studied in recent years. The human α7 subunit is approximately 50 kD in size and composed of 502 amino acids, including a 22 amino acid signal peptide. The protein may be divided into an extracellular N-terminal and a transmembrane domains. The N-terminal domain, composed of approximately 200 amino acids forming 10 β strands, encompasses the ligand-binding domain. The transmembrane domain comprises four α helices crossing the lipid bilayer and constitutes the ion channel. The α7 nAChR is highly permeable to Ca^{2+} ions and is therefore characterized as a calcium channel. Agonist binding leads to conformational changes via a quaternary symmetrical twist, opening the hydrophobic gate and allowing passage of ions. Subsequent to activation, the α7 nAChR rearranges into desensitized state, resulting in loss of biological response.[2]

The three-dimensional structure of the homopentameric human α7 nAChR has not been resolved at the atomic level. However, information obtained from photoaffinity labeling,[3] site-directed mutagenesis, and electron microscopy studies for this member of the nAChR family has provided significant insight about this receptor's 3D characteristics. Further, high resolution X-ray structures are available for several acetylcholine binding proteins (AChBP),[4] water-soluble homologues of the extracellular domain for nAChR, either free or in complex with known nAChR ligands.[5] Recently, crystal structures of the extracellular domain of a chimeric receptor, constructed from the α7 nAChR and SChBP, have been resolved.[6] Comparative modeling studies of nAChR proteins and ligand docking into the derived homology models have provided new avenues for understanding the molecular recognition process in these systems, facilitating the design of more potent and selective ligands.[7] Likewise, ligand-based pharmacophore modeling studies have shown agreement with historical nicotinic choligernic pharmacophore models, in which a cationic center as a protonated amino group, and a hydrogen bond acceptor and/or π-electron moiety, are generally required for binding.[8]

The $\alpha7$ subunit is expressed at high levels in hippocampus and cerebral cortex, brain regions involved in learning and memory.[9] Accumulating physiological,[10] pharmacological,[11] and human genetic[12] experimental data suggest involvement of $\alpha7$ nAChR in the cognitive deficits associated with a number of neuropsychiatric and neurodegenerative diseases including schizophrenia and Alzheimer's disease. The growing body of evidence has highlighted the clinical need for the development of $\alpha7$ nAChR agonists, which may offer new approaches to the treatment of impaired cognitive functions.

Initial efforts in the design and discovery of selective $\alpha7$ nAChR agonists was both facilitated and hampered by observation that ligands can show dual affinity at both the 5-HT$_3$ receptor (5-HT$_3$R) and nAChR.[13] The 5-HT$_3$R and nAChRs are both members of the Cys-loop superfamily of ligand-gated ion channels. Further, there is significant sequence homology between 5-HT$_3$R and $\alpha7$ nAChR in the ligand recognition domain.[14] Previously reported potent $\alpha7$ nAChR agonists[15] lacked selectivity versus 5-HT$_3$R,[16] and antagonist activity at 5-HT$_3$R often translated into agonism at $\alpha7$ nAChR. The crossover in affinity might be explained by commonly shared pharmacophoric elements for both 5-HT$_3$R and $\alpha7$ nAChR: a basic amine (protonated at physiological pH) provides for a cation−π interaction, a hydrogen-bond acceptor, e.g., a carbonyl group, forms a hydrogen bond, and aromatic moieties participate in π−π interactions.[17] In view of reported side effects, i.e., constipation, asymptomatic electrocardiogram changes and arrhythmias associated with 5-HT$_3$R antagonists,[18] our efforts were focused on design of ligands specifically interacting with only the $\alpha7$ nAChR to maximize the therapeutic effect and minimize the adverse effects.

Approaches to design selective $\alpha7$ nAChR agonists as reported in the literature (for most recent review, see Mazurov et al.[19]) are generally focused on modifying the aromatic moiety in 3-substituted quinuclidines. Such methodology is attractive, mostly because of the straightforward chemistry, and resulted in a few relatively selective clinical drug candidates, e.g., PHA-543613,[20] PHA-568487,[21] ABT-107,[22] and AZD0328[23] (Figure 1). Unfortunately, these chemical entities were discontinued after phase 1 clinical trials due to various adverse effects. Instead of gradual modification of the established pharmacophoric elements, we explored the alternative by incorporating a novel moiety into the azabicyclic scaffold. Synthetic pharmacophore directed diversification around the quinuclidine scaffold through exploration of both positions 2 and 3 (Figure

2) led us to discovery of 2-(pyridin-3-ylmethyl)quinuclidine amide series. Besides the three pharmacophoric elements
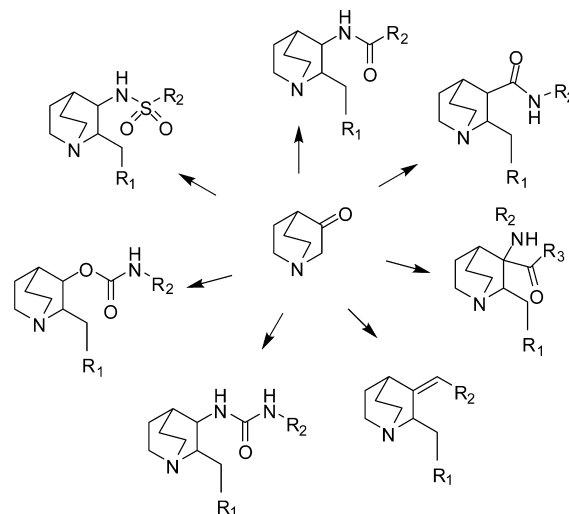

Figure 2. Diversification around quinuclidine scaffold via exploration of positions 2 and 3.

common to 5-HT$_3$R and $\alpha7$ nAChR, an additional, essential pharmacophoric element in the form of a hydrogen bond acceptor (pyridin-3-yl) in position two of azabicyclic ring, was revealed. The molecular basis of how the introduction of the 2-(pyridin-3-yl) group may trigger specificity toward $\alpha7$ nAChR over 5-HT$_3$R has been explained by our computational studies and will be discussed later in the text.

Herein, we detail the synthesis, molecular modeling, and pharmacological profile of the series of 2-(pyridin-3-ylmethyl)-quinuclidine amides, leading to the discovery of (2S,3R)-N-[2-(pyridin-3-ylmethyl)-1-azabicyclo[2.2.2]oct-3-yl]benzo[b]-furan-2-carboxamide (TC-5619, **7a**). To unravel the binding mode of **7a** into its cognate protein human $\alpha7$ nAChR, we have used homology modeling, molecular docking, and pharmacophore elucidation techniques.

■ CHEMISTRY

The 3-substituted 1-azabicyclo[2.2.2]octane has proved to be a convenient scaffold for generation of potent $\alpha7$ nAChR agonists with stereochemical preference at the position 3 for the R-enantiomer.[24] While asymmetric hydrogenation of prochiral ketones has been successfully demonstrated for conversion of quinuclidin-3-one into the enantiomerically pure amine,[25] asymmetric synthesis of 2-substituted 3-amino-1-azabicyclo[2.2.2]octane with two stereogenic centers has not been reported in the literature. Incorporation of two asymmetric centers into molecule during the lead optimization process requires development of the synthesis with controlled stereoconfiguration of target compounds to facilitate SAR and potential development of a drug candidate. The asymmetric synthesis was implemented in five steps starting from prochiral 1-azabicyclo[2.2.2]octan-3-one (Scheme 1). 2-(Pyridin-3-yl-methyl)-1-azabicyclo[2.2.2]octan-3-one (**3**) was prepared by aldol condensation of commercially available quinuclidin-3-one (**1**) with 3-pyridinecarboxaldehyde to afford the enone **2**, followed by catalytic hydrogenation. Racemizable ketone **3** was converted into its (2S)-enantiomer **4** by dynamic kinetic asymmetric transformation. Screening of chiral acids resulted in selection of di-p-toluoyl-D-tartaric acid as an optimal resolving
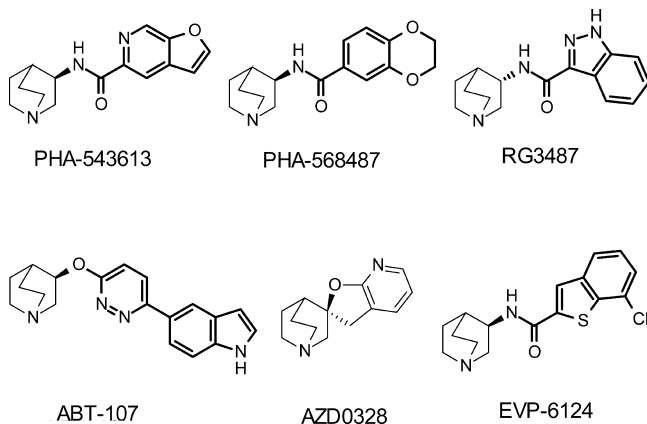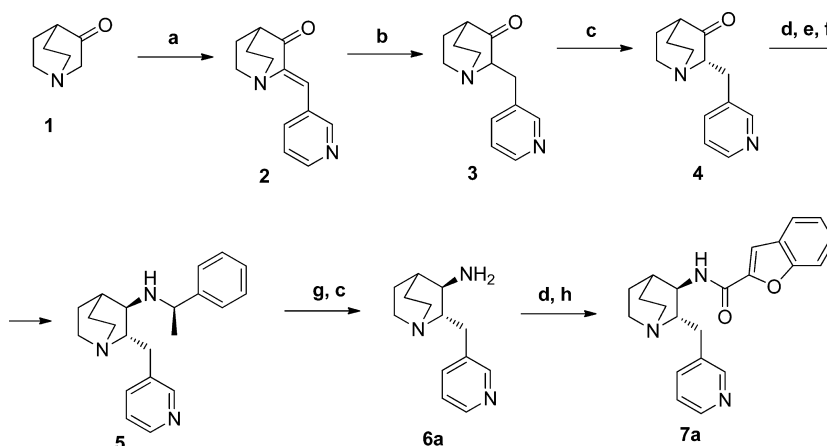

PHA-543613   PHA-568487   RG3487

ABT-107   AZD0328   EVP-6124

Figure 1. $\alpha7$ nAChR agonists: clinical drug candidates.

Scheme 1[a]

[a]Reagents and conditions: (a) 3-pyridinecarboxaldehyde, KOH/methanol; (b) H$_2$, Pd/C; (c) (+)-*O,O'*-di-*p*-toluoyl-D-tartaric acid; (d) NaHCO$_3$; (e) *R*-(+)-methylbenzylamine, Ti(Oi-Pr)$_4$; (f) NaBH$_4$; (g) cyclohexene, Pd/C; (h) benzo[*b*]furan-2-carboxylic acid, HBTU.

agent. Heating of ketone **3** in ethanol in the presence of the chiral acid provided sufficiently pure for the next step diastereomeric salt of (2*S*)-2-(pyridin-3-ylmethyl)-1-azabicyclo-[2.2.2]octan-3-one (**4**). A second stereogenic center was introduced by stereoselective reductive amination in the presence of α-methylbenzylamine and titanium isopropoxide. Selective cleavage of α-methylbenzyl group without reduction of pyridine moiety was achieved by transfer hydrogenation of **5** using cyclohexene to obtain (2*S*,3*R*)-3-amino-2-(pyridin-3-ylmethyl)-1-azabicyclo[2.2.2]octane (**6a**). Quinuclidine amides were readily synthesized by the coupling of enantiomerically pure amine **6a** (Scheme 1) with carboxylic acids. The above-described synthesis of (2*S*,3*R*)-*N*-[2-(pyridin-3-ylmethyl)-1-azabicyclo[2.2.2]oct-3-yl]benzo[*b*]furan-2-carboxamide (**7a**) has been used to produce kilogram quantities of the material without chromatographic purifications.

To obtain (2*R*,3*S*)-*N*-[2-(pyridin-3-ylmethyl)-1-azabicyclo-[2.2.2]oct-3-yl]benzo[*b*]furan-2-carboxamide (**7b**), ketone **3** was converted into diastereomeric mixture **6** via reductive amination (Scheme 2), followed by fraction crystallization of di-*p*-toluoyl-L-tartrate and coupling **6b** with benzo[*b*]furan-2-carboxylic acid. (2*R*,3*R*)-*N*-[2-(Pyridin-3-ylmethyl)-1-azabicyclo[2.2.2]oct-3-yl]benzo[*b*]furan-2-carboxamide (**7c**) and (2*S*,3*S*)-*N*-[2-(pyridin-3-ylmethyl)-1-azabicyclo[2.2.2]oct-3-yl]benzo[*b*]furan-2-carboxamide (**7d**) were isolated by

Scheme 2[a]
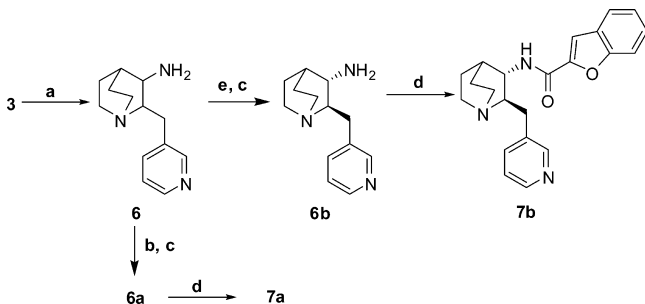
[a]Reagents and conditions: (a) HCO$_2$NH$_4$, ZnCl$_2$/ether, NaCNBH$_3$; (b) (+)-*O,O'*-di-*p*-toluoyl-D-tartaric acid; (c) NaOH; (d) benzo[*b*]-furan-2-carboxylic acid, HBTU; (e) (−)-*O,O'*-di-*p*-toluoyl-L-tartaric acid.

preparative chiral HPLC as side products during synthesis of **7a**.

■ RESULTS AND DISCUSSION

When we started our α7 nAChR drug discovery program, previously reported 3-substituted quinuclidine aryl amides (for example, **8**) were dual 5-HT$_3$R and α7 nAChR ligands,[16,26] while 2-substituted pyridin-3-yl quinuclidines (for example, **9** and **10**) interacted with multiple nAChRs (Figure 3).[27] The
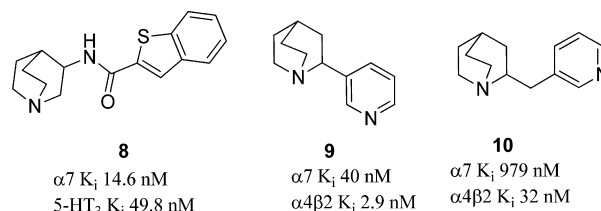

8
α7 K$_i$ 14.6 nM
5-HT$_3$ K$_i$ 49.8 nM

9
α7 K$_i$ 40 nM
α4β2 K$_i$ 2.9 nM

10
α7 K$_i$ 979 nM
α4β2 K$_i$ 32 nM

Figure 3. Quinuclidine containing nonselective nAChR ligands.

quinuclidine scaffold provides an essential α7 nAChR pharmacophoric element; its basic nitrogen, occupying a bridgehead position within an azabicyclic system, allocates maximal electrostatic interaction combined with minimal steric demand.

Generally, relatively small groups (methyl)[28] or large ones (benzyl)[29] in the position 2 of the azabicyclic ring reduce nAChR affinity. Incorporation of the (pyridin-3-yl)methyl moiety at the position 2 adjacent to the position 3 amide bond drastically modified the pharmacological profile, resulting in improved selectivity (especially over 5-HT$_3$R), increased α7 nAChR affinity (about 1 order of magnitude) and potency, eliminated hERG inhibition, and enhanced microsomal stability of the series. Among aromatic carbocyclic and heteroaromatic rings, pyridin-3-yl was an optimal potential hydrogen bond acceptor, providing specific interaction with α7 nAChR. To evaluate 2-(pyridin-3-ylmethyl)quinuclidine amides for our α7 nAChR program, small focused libraries of amides were designed and synthesized based on readily accessible chiral amine **6a**, which contains two stereogenic centers. Conjugation of the latter with aromatic carboxylic acids provided several series of compounds for potential development. Three structural series were investigated and are described herein:

Table 1. Affinity and Agonism of Benzamides
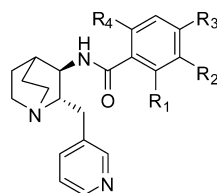
compd	R_1	R_2	R_3	R_4	human $\alpha7$ K_i (nM)	$\alpha7$ EC_{50} (μM)	$\alpha7$ E_{max} (%)	human $\alpha4\beta2$ K_i (nM)
nicotine					3000 ± 400	23 ± 1.5	103 ± 4	2 ± 0.2
11	H	H	H	H	97 ± 27	1.1 ± 0.3	79 ± 3	2000 ± 200
12	F	H	H	H	500 ± 46	3.0 ± 1.2	45 ± 3	1300 ± 100
13	H	F	H	H	$29.1^{a,b}$	411 ± 45	47 ± 3	900 ± 100
14	H	H	F	H	31 ± 14	0.7 ± 0.1	47 ± 3	700 ± 200
15	Cl	H	H	H	2156 ± 292	2.3 ± 0.4	24 ± 5	1200 ± 400
16	H	Cl	H	H	46 ± 5	0.6 ± 0.4	97 ± 4	500 ± 300
17	H	H	Cl	H	15 ± 3	0.2 ± 0.05	35 ± 2	1400 ± 100
18	H	H	Br	H	6.2 ± 0.6	0.06 ± 0.04	56 ± 5	900 ± 100
19	H	H	NMe_2	H	112 ± 20	0.7 ± 0.1	80 ± 3	300 ± 100
20	H	H	OMe	H	6.4 ± 1.0	0.06 ± 0.01	25 ± 3	900 ± 100
21	H	H	OH	H	$94.8^{a,b}$	0.4 ± 0.07	34 ± 4	1600 ± 300
22	H	H	CH_2OH	H	76 ± 6	1.0 ± 1.3	92 ± 6	1100 ± 400
23	H	F	OH	H	52.5 ± 4.2	1.7 ± 0.8	32 ± 3	4400 ± 300
24	Cl	H	Cl	H	851 ± 631	7.1 ± 1.8	79 ± 4	1200 ± 200
25	H	Cl	Cl	H	20 ± 4	0.3^a	22^a	600 ± 10
26	F	H	OMe	F	150 ± 15	0.6 ± 0.1	17 ± 5	900 ± 100
27	H	OCH_2CH_2O		H	24.1 ± 5.3	0.11^a	50^a	2300 ± 300

^{a}n = 1. ^{b}Rat $\alpha7$ K_i.

Table 2. Affinity and Agonism of Heteroaryl Amides
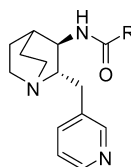
compd	R	human $\alpha7$ K_i (nM)	$\alpha7$ EC_{50} (μM)	$\alpha7$ E_{max} (%)	human $\alpha4\beta2$ K_i (nM)
28	pyridin-3-yl	1803 ± 403	3.3 ± 0.4	15 ± 3	500 ± 100
29	pyridin-2-yl	94 ± 16	0.65^a	87^a	200 ± 30
30	pyridin-4-yl	961 ± 140	4.8 ± 2.8	110 ± 12	1500 ± 200
31	3-Cl-pyridin-2-yl	$398^{a,b}$	ND^c	ND	>5000
32	4-Cl-pyridin-2-yl	60 ± 10	0.5 ± 0.2	66 ± 3	400 ± 100
33	5-Cl-pyridin-2-yl	30.0 ± 3.1	0.27 ± 0.06	72 ± 5	140 ± 70
34	6-Cl-pyridin-2-yl	219 ± 20	4.1 ± 0.5	81 ± 15	500 ± 100
35	quinolin-2-yl	168 ± 36	0.23 ± 0.05	62 ± 4	600 ± 100
36	quinolin-8-yl	$9574^{a,b}$	ND	ND	500 ± 30
37	isoquinolin-1-yl	2027 ± 374	ND	ND	1600 ± 300
38	isoquinolin-3-yl	2.8 ± 0.5	0.05 ± 0.01	52 ± 6	200 ± 80
39	5-Me-fur-2-yl	240 ± 70	11 ± 5	59 ± 6	2100 ± 400
40	4-Cl-fur-2-yl	66.2 ± 13.3	1.2 ± 0.6	70 ± 6	1400 ± 300
41	3-Br-fur-2-yl	6.2 ± 1.0	0.2 ± 0.3	77 ± 15	1500 ± 100
42	5-Br-fur-2-yl	56.3 ± 27.4	1.2 ± 0.1	38 ± 1	500 ± 200
43	5-(pyridin-2-yl)-fur-2-yl	705 ± 41	0.85 ± 0.49	15 ± 2	3300 ± 1000
44	5-phenyl-fur-2-yl	5.9 ± 1.9	0.16 ± 0.24	32 ± 5	3600 ± 400
45	isoxazol-3-yl	1097 ± 425	~10	10 ± 1	2100 ± 700
46	5-phenylisoxazol-3-yl	87.7 ± 34.6	>10	~50	2300 ± 800
47	styryl	4.3 ± 0.8	0.014 ± 0.02	42 ± 7	900 ± 100
48	2-(3-methylthien-2-yl)ethenyl	4.5 ± 0.3	0.014 ± 0.007	24 ± 5	400 ± 30

^{a}n = 1. ^{b}Rat $\alpha7$ K_i. ^{c}ND: not determined.

Table 3. Affinity and Agonism of Thiophenecarboxamides
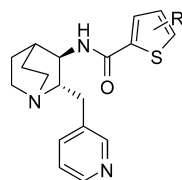
compd	R	human $\alpha 7$ K_i (nM)	$\alpha 7$ EC$_{50}$ (μM)	$\alpha 7$ E_{max} (%)	human $\alpha 4\beta 2$ K_i (nM)
49	5-Me	3.0 ± 1.1	0.03 ± 0.01	31 ± 5	1300 ± 500
50	5-Br	1.1 ± 0.4	0.011 ± 0.005	21 ± 4	1000 ± 200
51	5-I	0.51 ± 0.05	~ 0.001	~ 5	200 ± 20
52	5-Ph	0.8 ± 0.3	0.13 ± 0.04	16 ± 3	900 ± 100
53	4-Ph	$26.3^{a,b}$	0.39 ± 0.07	17 ± 3	1500^a
54	5-(pyridin-2-yl)	0.9 ± 0.2	0.03 ± 0.01	13 ± 5	1300 ± 300
55	5-(thien-2-yl)	1.2 ± 0.1	0.001 ± 0.002	13 ± 1	600 ± 30

$^a n = 1$. ^{b}Rat $\alpha 7$ K_i.

benzamides (Table 1), heteroaryl amides (Tables 2, 3), and derived from them benzofurancarboxamides (Tables 4, 5). All compounds shown in Tables 1−5 were evaluated for affinity to the $\alpha 7$ and $\alpha 4\beta 2$ binding sites in epibatidine and nicotine binding assays and for functional activity at the $\alpha 7$ subtype in the patch clamp electrophysiology assay.

The SAR of quinuclidine amide series (represented by **8**), as described in the literature, was driven mostly by optimization of $\alpha 7/5HT_3$ selectivity and improvement of hERG profile[20] without substantial loss of functional activity. Because the presence of pyridylmethyl moiety in quinuclidine amides eradicated those liabilities, our program objective was to identify clinical drug candidate with high in vitro functional and binding activity, with favorable in vivo efficacy as well.

In the benzamides series (Table 1), substitution of position four by electron withdrawing or electron donating group moderately affects affinity of the parent compound **11**, while meta- and especially ortho- substituents are detrimental to affinity and/or agonism. These observations corroborate our previous work[29] and the finding reported by Pharmacia (Pfizer) researchers.[30] Most of the benzamides are partial agonists with potency (EC$_{50}$) around 1 μM or less; p-bromobenzamide **18** and p-methoxybenzamide **20** are the most potent partial agonists in the series, with EC$_{50}$ values of 60 nM. Most heteroaromatic carboxamides demonstrate lower affinity to $\alpha 7$ nAChR (Table 2); however, the nature and position of the heteroatom play a crucial role in the interaction of the ligand with $\alpha 7$ nAChR. While para-substitution is most favorable in benzamides, location of an electronegative nitrogen atom in position 2 (compound **29**) is optimal for pyridinecarboxamides. In fact, compound **29** exhibits stronger binding affinity to $\alpha 7$ nAChR (K_i = 94 nM) as compared to its counterparts, compounds **30** (K_i = 964 nM) and **28** (K_i = 1800 nM). Benzamide **11** and pyridine-2-carboxamide **29** are equally potent $\alpha 7$ nAChR agonists, while the latter is less selective over $\alpha 4\beta 2$ nAChR. Binding experiments reflect interaction of the ligand with desensitized state of the $\alpha 7$ nAChR, whereas functional data provide information about active open channel. The latter is considered to be important for advancement of selective nAChR agonists to clinical trials.[20,31] Differences in affinity versus potency and efficacy might be explained by changing conformation of the receptor. Affinities of pyridine-2-carboxamides vary depending on the position of substituent (Table 2, compounds **31−34**). Location of the chlorine atom in the para-position relative to the carbonyl group seems to be

optimal for both benzamides and pyridinecarboxamides, providing essentially equivalent $\alpha 7$ K_i values for compounds **17** and **33**. However, compound **33** demonstrated low selectivity for $\alpha 7$ over $\alpha 4\beta 2$ nAChR, making this compound less attractive for further development. Extension of the π-system by incorporation of a covalently bound additional aromatic ring (compounds **43** and **44**), a fused aromatic system with an appropriate location of the heteroatom (compound **38**), or an alkene chain (compounds **47**, **48**) enhances the affinity for the $\alpha 7$ subtype. Furthermore, incorporation of the polarizable and relatively bulky bromine atom also increases binding as well (compounds **41**, **42**). In addition to the established arrangement of carboxamide moiety and aromatic nitrogen in pyridinecarboxamide **33**, the position of a fused aromatic ring appears to be essential as well. Modification from the pyridinecarboxamide (**33**) to the isoquinoline carboxamide (**38**) gave one of the most potent $\alpha 7$ nAChR partial agonists (10-fold increase in affinity), with approximately 100-fold selectivity over the $\alpha 4\beta 2$ subtype.

Replacement of a furan ring with thiophene (see for comparison compounds **39** and **49**) improves the affinity at least 1 order of magnitude, giving rise to the hypothesis that sulfur's d-orbital may provide enhanced interaction with $\alpha 7$ nAChR. Comparative docking studies of furan and thiopene derivatives **39** and **49** did not provide an explanation for their difference in affinity and potency. Given the identical docking poses obtained, the only difference between the two molecules is the replacement of oxygen atom with the more polarizable and bigger sulfur atom. Different electronic properties of the latter are usually explained by the presence of the d-orbital. To understand the molecular basis of such affinity enhancement, we have computed the hydrophilic/hydrophobic surface area of the binding site of the a7 nAChR homology model and the ligands, as described in the Experimental Section. The results obtained for the binding site are shown in Supporting Information Figure S2. We found that the hydrophilic and hydrophobic surface areas obtained were 1076.2 and 359.1 Å^2, respectively. The 3D-derived molecular polar solvent-accessible surface area values for compounds **49** and **39** were equal to 93.9 and 55.4 Å^2, respectively. Thus, hydrophilic complementarity (polar/polar) between the ligand and the binding site might explain the increase in binding affinity observed when furan is substituted with thiophene. Given the uniqueness of thiophenecarboxamides, a small focused library (Table 3) was prepared in spite of the propensity of thiophenes to undergo

Table 4. Affinity and Agonism of Benzofurancarboxamides
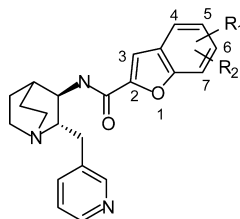
compd	R_1	R_2	human $\alpha7$ K_i (nM)	$\alpha7$ EC$_{50}$ (μM)	$\alpha7$ E_{max} (%)	human $\alpha4\beta2$ K_i (nM)
56	5-Cl	H	3.8 ± 0.9	0.06 ± 0.01	50 ± 6	1000 ± 300
57	5-Br	H	11.2 ± 4.8	0.1 ± 0.01	77 ± 2	1200 ± 400
58	5-OMe	H	2.1 ± 0.3	0.1 ± 0.01	45 ± 3	500 ± 100
59	7-OMe	H	5.9 ± 1.1	0.012 ± 0.005	13 ± 3	830 ± 140
60	7-OEt	H	22.1^a	ND^b	ND	1600^a
61	3-Me	H	2.2 ± 0.3	0.05^a	36^a	400 ± 100
62	5-Me	H	5.0 ± 1.1	0.09 ± 0.1	22 ± 3	620 ± 60
63	6-Me	H	5.5 ± 0.7	0.11 ± 0.01	78 ± 5	1500 ± 200
64	5-OH	H	1.8 ± 0.8	0.03 ± 0.01	16 ± 2	740 ± 350
65	5-F	H	4.7 ± 0.9	0.05 ± 0.01	19 ± 4	1300 ± 400
66	3-Me	5-F	12.3 ± 5.2	0.05 ± 0.03	13 ± 4	1300 ± 200
67	3-Me	7-F	33.8 ± 1.9	0.11^a	59^a	1100 ± 400
68	3-Me	5-Me	15.7 ± 4.7	0.5^a	75^a	330 ± 160
69	3-Me	5-Cl	11.5 ± 3.9	0.12 ± 0.08	10	1000 ± 200
70	3-Me	7-Cl	352 ± 127	8.2 ± 0.8	24 ± 4	980 ± 140
71	3-OMe	5-Cl	36.1 ± 10.0	1.5 ± 0.19	79 ± 13	760 ± 120
72	5-Cl	7-Br	259 ± 65	0.96 ± 0.1	78 ± 4	1300 ± 500
73	7-(2-OMe-phenyl)	H	59 ± 6	0.14^a	46^a	9000 ± 3400
74	7-(pyridin-2-yl)	H	29 ± 6	0.28 ± 0.2	42 ± 6	5100 ± 2100

$^a n = 1$. ^{b}ND: not determined.

Table 5. N-[2-(Pyridin-3-ylmethyl)-1-azabicyclo[2.2.2]oct-3-yl]benzo[b]furan-2-carboxamide Stereomers
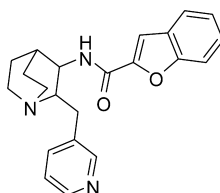
compd	configuration	$[\alpha]^{25}_{589}$ $c = 1$, water	human $\alpha7$ K_i (nM)	$\alpha7$ EC$_{50}$ (nM)	$\alpha7$ E_{max} (%)	human $\alpha4\beta2$ K_i (nM)
7a	2S,3R	-13.87^a	1.40 ± 0.35	17 ± 5	76 ± 5	1700 ± 800
7b	2R,3S	$+15.35^a$	413 ± 80	140 ± 13	25 ± 2	8000 ± 2300
7c	2R,3R	-94.51^b	4.98 ± 1.29	20 ± 7	20 ± 13	157 ± 28
7d	2S,3S	$+116.70^b$	818 ± 313		0	1200 ± 400

^{a}p-Toluenesulfonate. ^{b}Galactarate.

cytochrome P450-catalyzed bioactivation to electrophilic intermediates, which might form covalent bonds with bioorganic nucleophiles and elicit a toxicological response.[32] Because drugs containing a thiophene ring are hydroxylated by cytochrome P450 on the carbon atoms adjacent to sulfur,[33] formation of the electrophilic thiophene-2,3-epoxide is likely impeded by blockade of positions 2 and 5, especially by electron-withdrawing substituent as carboxamide group. Most compounds of this series were obtained from 5-substituted thiophene-2-carboxylic acids. For $\alpha7$ nAChR function, efficacy of thiophene-2-carboxamides (Table 3) does not exceed 30% despite their high potency and affinity. Given subnanomolar affinity and selectivity, compounds 51 and 55 are being considered for development as radioligands.

A broad range of pharmacological profiles (both binding and function) were observed for benzofuran-2-carboxamides (Table 4). Most compounds of this series are more efficacious than thiophenecarboxamides agonists, with potency below 1 μM. Small substituents around the benzofuran ring were well tolerated, while 7-aryl substituted compounds 73 and 74 gave somewhat lower affinity, still demonstrating very potent partial agonism at the $\alpha7$ nAChR subtype with negligible binding to the $\alpha4\beta2$ subtype. Disubstituted benzofurancarboxamides do not appear to improve the pharmacological profile of the series.

Generally, 2-(pyridin-3-ylmethyl)quinuclidine amides interact weakly with 5-HT$_3$R (Table 6) and do not possess significant hERG (human ether-à-go-go related gene) potassium channel activity (Table 7). Those characteristics indicate an improved safety profile over 2-unsubstituted quinuclidine

Table 6. Human 5-HT$_3$R Affinity of Selected Compounds

compd	% inhibition at 10 μM (K_i, μM)
7a	25
14	15
38	39 (18.6)
42	14
49	20
54	12
56	22
7b	20

Table 7. hERG Inhibition of Selected Compounds

compd	% inhibition at 10 μM (IC$_{50}$, μM)
7a	(54)[a]
14	0.4 ± 1.1
27	0.1 ± 0.4
56	31.1 ± 1.3
61	20.4 ± 1.2
65	2.6 ± 0.9
66	6.0 ± 0.8
67	2.8 ± 0.6
68	5.1 ± 0.5

[a]IC$_{50}$ value

amides and in combination with high potency provide an avenue toward further development.

Compound **7a**, the parent compound of the benzofurancarboxamide series (Table 5), was a highly potent α7 nAChR agonist and was selected for further profiling. In vitro pharmacological profiles were obtained and evaluated for all four isolated stereoisomers of *N*-[2-(pyridin-3-ylmethyl)-1-azabicyclo[2.2.2]oct-3-yl]benzo[*b*]furan-2-carboxamide. Stereoisomers **7a** and **7c** (possessing a (3*R*)-configuration) are the most potent known α7 nAChR agonists, with EC$_{50}$ values of 17 and 20 nM, respectively. The (2*S*,3*R*)-enantiomer **7a** was found to be much more efficacious, with an E_{max} of 76% compared to 20% for **7c**. (2*R*,3*S*)-Antipode **7b** was as efficacious as **7a** but

less potent. (2*S*,3*S*)-Enantiomer **7d** showed moderate affinity and did not activate the α7 nAChR. Absolute configurations of compounds **7a** (Figure 4) and **7c** (Figure 5) were determined by X-ray crystallographic analysis, elucidating the stereochemistry of their antipodes **7b** and **7c**.
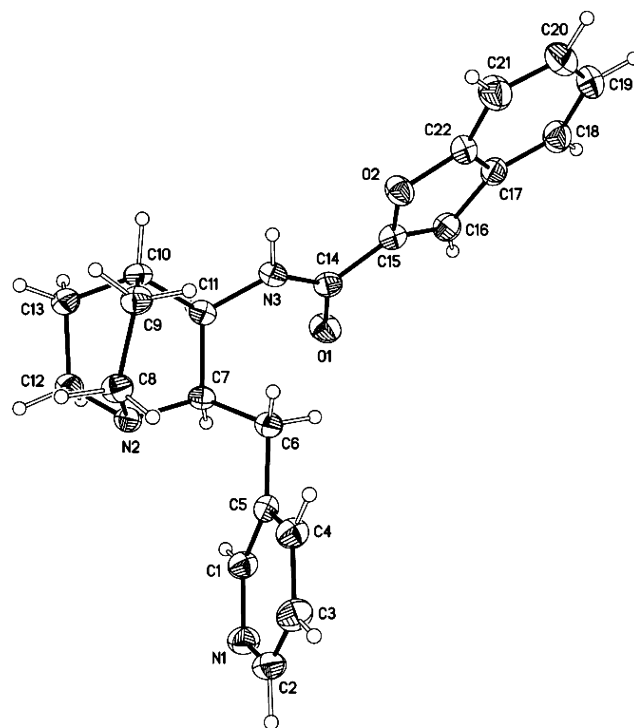

Figure 5. A view of a molecule of (2*R*,3*R*)-*N*-[2-(pyridin-3-ylmethyl)-1-azabicyclo[2.2.2]oct-3-yl]benzo[*b*]furan-2-carboxamide (**7c**) as a free base from the crystal structure showing the numbering scheme employed. Anisotropic atomic displacement ellipsoids for the non-hydrogen atoms are shown at the 50% probability level. Hydrogen atoms are displayed with an arbitrarily small radius.
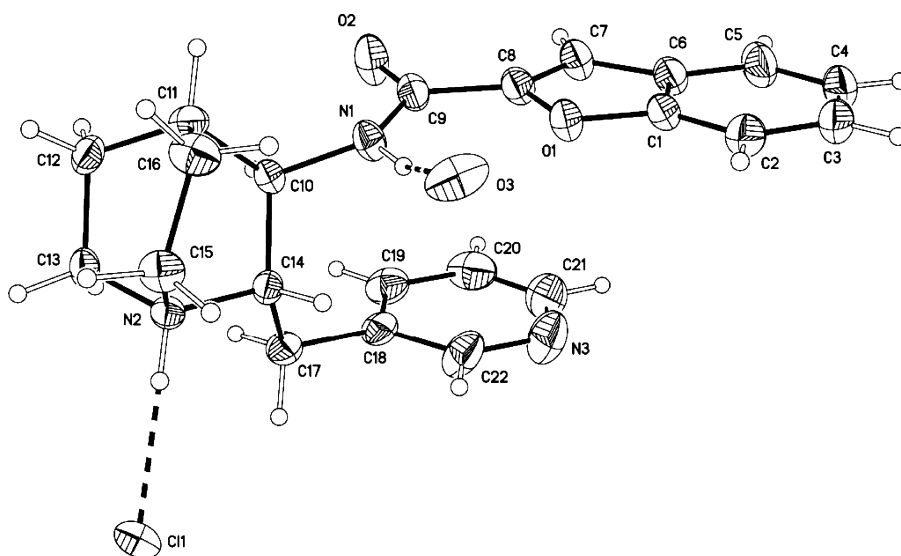

Figure 4. A view of a molecule of (2*S*,3*R*)-*N*-[2-(pyridin-3-ylmethyl)-1-azabicyclo[2.2.2]oct-3-yl]benzo[*b*]furan-2-carboxamide (**7a**) as the partially hydrated hydrochloride salt from the crystal structure showing the numbering scheme employed. Anisotropic atomic displacement ellipsoids for the non-hydrogen atoms are shown at the 50% probability level. Hydrogen atoms are displayed with an arbitrarily small radius.

7a is an agonist at $\alpha7$ nAChR with a high binding affinity to membrane preparations from both rat brain (0.42 ± 0.07 nM) and in a HEK293 cell line coexpressing human $\alpha7$ nAChR and RIC3 cDNAs. With more than a thousand-fold separation, **7a** displayed a K_i of 2.8 μM at $\alpha4\beta2$ nAChR expressed in SH-EP1 cellular membranes and a K_i of 2.1 μM at $\alpha4\beta2$ nAChR expressed in rat cortical membranes. **7a** has no detectable effects on muscle or ganglionic nicotinic receptor subtypes, indicating a marked selectivity for the CNS over the PNS. To determine proteomic selectivity profile for non-nicotinic receptor classes, **7a** and ten of its analogues were tested in 64 bioassays at 10 μM concentration. Binding of **7a** (10 μM) to 5-HT$_3$R displayed 59% inhibition of radioligand binding at the mouse receptor and 25% inhibition at the human receptor, demonstrating good selectivity for the $\alpha7$ nAChR. Investigation of functional activation at the mouse 5-HT$_3$R suggested minimal to no activation; a maximal response of 15% was obtained at 100 μM of **7a**. Compounds **7a**, **7b**, and **56** showed greater than 50% inhibition to the sodium channel, site 2. No inhibition of xenobiotic drug-metabolizing enzymes cytochrome P450 was observed. On the whole, **7a** appears to have very little off-target activity.

Pharmacokinetic evaluations of **7a** have included in vivo studies in rats and dogs and in vitro assessments of permeability, metabolism, potential to inhibit and induce various drug metabolizing enzymes, and potential to inhibit transporters. In nonclinical pharmacokinetic studies in the rat, **7a** showed oral bioavailability of approximately 20−40% and a half-life of about 2−3 h. Distribution of **7a** specifically to the brain has been assessed using the relative concentration differences between the brain and the plasma in rats. The brain−plasma concentration ratio (0.4 at 6h) was evaluated and increased with time after administration of the compound, indicating a slower rate of elimination from the brain than from plasma. **7a** exhibits concentration-independent low to moderate binding to plasma proteins in human, rat, guinea pig, mouse, and monkey plasma. The highest degree of binding was observed in human plasma. About 60% of **7a** was bound to plasma proteins with preference to α_1-acid glycoprotein over human serum albumin. Incubation in vitro to evaluate **7a** metabolism revealed less than 25% decline in human liver microsomes at 60 min and 27% decline in human hepatocytes at 4 h. **7a** is a potential substrate for several drug-metabolizing enzymes including CYP3A4, CYP2C19, CYP2E1, and FMO, with CYP3A4 predominating. It does not induce CYP1A2, CYP2B6, or CYP3A4 at concentrations up to 10 μM and does not inhibit CYP450 of the major drug-metabolizing enzymes at concentrations up to 100 μM. In summary, **7a** demonstrated a favorable in vivo and in vitro metabolism and pharmacokinetic profile with a low potential for clinically relevant drug−drug interactions in human.

7a has positive effects across a variety of animal models testing cognitive function as well as positive and negative symptoms of schizophrenia.[34] **7a** demonstrated significant enhancement of short-term working memory in the novel object recognition paradigm over a wide dose range. Moreover, effects on memory were seen up to 18 h following oral administration, suggesting a positive effect on long-term memory consolidation as well. In addition to the cognitive-enhancing properties, **7a** also reversed apomorphine-induced prepulse inhibition both in mice and rats as a preclinical model of positive symptoms of schizophrenia. The positive effects of **7a** in the social withdrawal model in mice indicate that the

compound has the potential to target negative symptoms of the disease. Its effects appear to be additive or synergistic with the antipsychotic clozapine, further supporting the therapeutic potential of the compound not only as monotherapy but also as add-on therapies in combination with existing drugs. These results suggest that **7a** has therapeutic potential for the treatment of symptomatic domains of schizophrenia and other cognitive impairments caused by cholinergic dysfunction. Compound **7a**, used as an augmentation therapy to the standard treatment with antipsychotics, demonstrated encouraging results on measures of negative symptoms and cognitive dysfunction in schizophrenia and was well tolerated in a phase II clinical proof of concept trial in patients with schizophrenia.[35]

Molecular Modeling. In attempt to better understand the molecular basis of the binding selectivity of compound **7a** toward $\alpha7$ nAChR vs $\alpha4\beta2$ nAChR and 5HT$_{3A}$, we have carried out a detailed analysis of the predicted binding modes of this compound to these receptors subtypes. As a control, we have performed a comparative study for (3R)-7-chloro-N-quinuclidin-3-yl)benzo[b]thiophene-2-carboxamide (EVP-6124, **75**),[36] a dual $\alpha7$ nAChR and 5HT$_{3A}$ receptor ligand. Figure 6 shows the best docked pose of compound **7a** into the $\alpha7$ nAChR subtype 3D model. The ligand basic nitrogen atom donates hydrogen bonds to the backbone carbonyl oxygen atom of the highly conserved Trp-148, of the principal face. Moreover, the
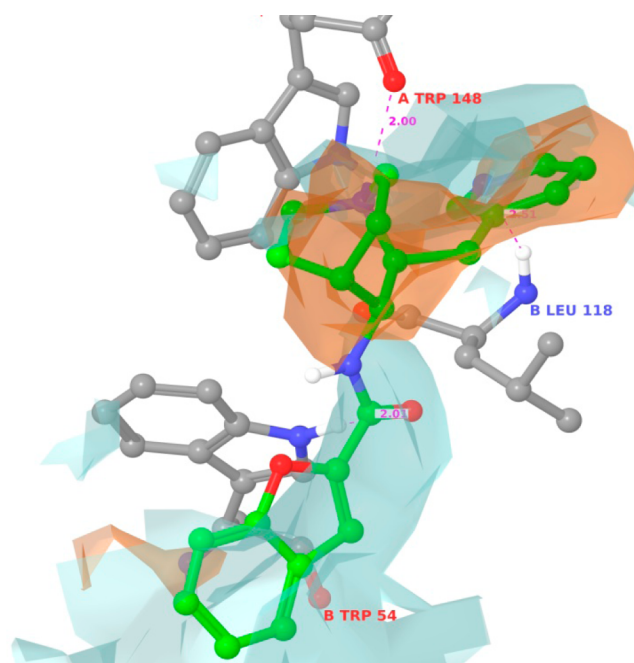

Figure 6. Best pose obtained for compound **7a** docked into the binding site of the human $\alpha7$−AChBP chimera crystal structure. The docked ligand is shown in ball and stick and colored green. Trp-54 and Leu-118 (of the complementary face) and the highly conserved Trp-148 (of the principal face), which are involved in hydrogen-bonding interactions with compound **7a**, are also shown in ball and stick. The cationic center of the ligand donates a hydrogen bond to the backbone carbonyl group of the highly conserved Trp-148. The amide oxygen atom of the ligand accepts a hydrogen bond from the indole NH group of Trp-54, and the pyridine nitrogen accepts a hydrogen bond from the backbone NH group of Leu-118. All the hydrogen-bonding distances are shown in broken lines colored in magenta. Hydrophilic and hydrophobic surfaces are shown in light-blue and orange, respectively.
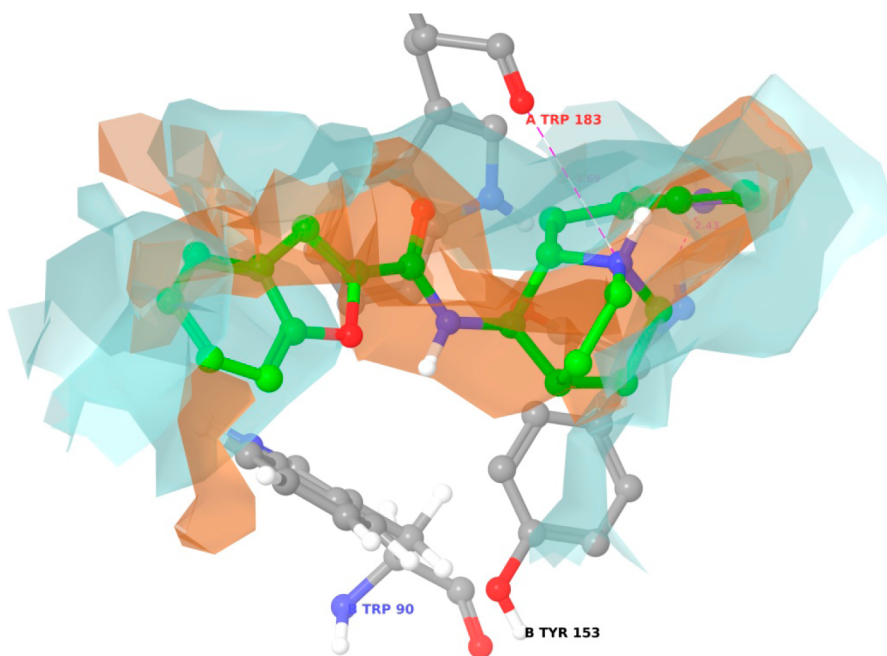
Figure 7. Best pose of compound **7a** docked into human 5HT$_{3A}$ homology model. The ligand is shown in ball and stick and colored green. The pyridine nitrogen atom accepts a hydrophobically packed hydrogen bond from the backbone nitrogen atom of Tyr-153 of the complementary face. Also shown in ball and stick are the highly conserved Trp-183 of the principal face and Trp-90 of the complementary face. The broken line indicates the distance between the cationic center and the backbone carbonyl oxygen atom of Trp-183, which measures 3.69 Å. Hydrophilic and hydrophobic surfaces are shown in light-blue and orange, respectively.

Table 8. Geometry and Energy Characterizing the Interaction between the Conserved Trp Residue Located at the Binding Site of α7, α4β2, 5HT$_{3A}$ and the Ligand

	α7 nAChR		α4β2 nAChR		5HT$_{3A}$R	
compd	acceptor−donor distance (Å)	per residue Coulomb−van der Waals interaction energy (kcal/mol) and K_i (nM)	acceptor−donor distance (Å)	per residue Coulomb−van der Waals interaction energy (kcal/mol) and K_i (nM)	acceptor−donor distance (Å)	per residue Coulomb−van der Waals interaction energy (kcal/mol) and K_i (nM)
7a	2.87	−9.97 [1.0]	2.70	−7.88 [1700]	3.69	−3.84 [> 10,000]
7S	2.75	−14.35 [9.98]	3.30	−6.47 [>10000]	3.00	−13.04 [51% inhibition at 10 nM]

ligand amide oxygen atom accepts a hydrogen bond from the side-chain NH group of Trp-54, of the complementary face. Furthermore, the nitrogen atom of the pyridin-3-ylmethyl group accepts a hydrogen bond from the backbone nitrogen atom of Leu-118, of the complementary face. In addition to the above-mentioned hydrogen-bonding interactions, cation−π interactions, pairwise lipophilic interactions, and hydrophobic enclosures significantly contribute to the binding affinity as indirectly predicted by the derived Glide score (data not shown).

Figure 7 indicates that the best pose obtained for compound **7a** docked into the 5HT$_{3A}$ protein homology model appears to be strikingly different. The nitrogen atom of the 2-(pyridin-3-yl) group accepts a hydrophobically packed hydrogen bond from the backbone NH group of Tyr-153 of the complementary face, and prevents the cationic center to make the quintessential hydrogen bond with the backbone carbonyl oxygen atom of the highly conserved Trp-183 (distance of 3.69 Å). As a result, the benzofuranyl residue drifts away from Trp-90 of the complementary face (the equivalent of Trp-54 in the α7 protein), which could have donated a hydrogen bond to the ligand amide oxygen atom.

Results summarized in Table 8 refer to the best docking poses obtained. For both compounds **7a** and **7S**, the protonated nitrogen atom of the ligand (which can act as a hydrogen bond donor) is in good hydrogen-bonding distance (2.75 and 2.87 Å, respectively) to the carbonyl oxygen atom of the conserved Trp of the α7 nAChR. Moreover, favorable strong interaction energy is observed between **7a** and **7S** and the conserved Trp residue for both molecules (−14.35 and −9.97 kcal/mol, respectively). Furthermore, compound **7a** does not contract such a hydrogen bond at the 5HT$_{3A}$ binding site (distance of 3.69 Å) but can make it at the α4β2 nAChR binding site (distance of 2.70 Å). By contrast, the cationic center of compound **7S** does not donate a hydrogen bond to the conserved Trp-149 at the α4β2 binding site (distance of 3.30 Å). Likewise, the selective compound SSR-180711[37] and the nonselective compound RG3487[38] exhibit a donor−acceptor distance of 4.84 and 2.58 Å, respectively, and an interaction energy of −11.13 and −15.10 kcal/mol, respectively, when docked into the 5HT$_3$ homology model. By contrast, the two compounds exhibit corresponding distances of 2.00 and 2.65 Å, respectively, and an interaction energy of −15.02 and −11.79 kcal/mol, respectively, when docked into the α7 homology model. This result further illustrates and supports the trend observed in Table 8, and the high ROC scores obtained when the homology models were validated. We also found that compound **7a** interacts minimally with Trp-183 of 5HT$_{3A}$ (interaction energy of −3.84 kcal/mol and K_i > 10000 nM) but slightly stronger with α4β2 (interaction energy

of −7.88 kcal/mol, and K_i = 1700 nM). These results suggest that the stronger (i.e., the more negative) the interaction energy (including van der Waals, Coulombic, and hydrogen-bonding involving the cationic center) between compound **7a** and the highly conserved Trp at the binding site of α7 nAChR (K_i = 1.0 nM), α4β2 nAChR (K_i = 1700 nM), and their homologue serotonergic ion channel 5HT$_{3A}$, the better the binding affinity between the ligand and these receptors subtypes. By contrast, we found that compound **75** interacts strongly with Trp-183 of 5HT$_{3A}$ (interaction energy of −13.04 kcal/mol and percent inhibition of 51% at 10 nM) but interacts minimally with Trp-149 of α4β2 (interaction energy of −6.47 kcal/mol and K_i > 10 uM). It is important to mention that it is the 2-[(pyridin-3-yl)methyl] group of **7a**, which provides the selectivity over 5HT$_3$ receptor. In fact, the loss of favorable interactions with the conserved Trp-183 may result from tipping the balance of interactions preferentially toward the strong hydrophobically packed hydrogen bond involving the pyridine group. By contrast, the hydrogen bond contracted by the 2-[(pyridin-3-yl)methyl] moiety, when **7a** interacts with α7 nAChR, is not hydrophobically packed. Thus, it is not strong enough to interfere with the interactions between the cationic center and the conserved Trp residue.

Distances and interaction energies were calculated from the best pose obtained after docking the ligand into the homology model of the receptor protein, built as described in Experimental Section. Distances shown are between the ligand cationic center and the carbonyl oxygen atom of the highly conserved Trp-148, Trp-149, and Trp-183 located at the binding site of α7 nAChR, α4β2 nAChR, and 5HT$_{3A}$ receptors, respectively. In each case, the per residue interaction energies (Coulomb + van der Waals) between the conserved Trp residue and the ligand is also shown. Experimentally observed K_i values expressed in nM and percent inhibition at 10 μM are shown in brackets. K_i values and percent inhibition for **75** were taken from Prickaerts et al.[36]

The 2-(pyridin-3-yl)methyl group is oriented such that the pyridine occupies the loop-E region of the receptor. In the X-ray crystal structure of nicotine-bound AChBP, the pyridine nitrogen interacts with the backbone carbonyl oxygen of Leu-102 as well as the amide NH of Met-114, in the complementary face, through a network of water-mediated hydrogen bonds.[39] Similarly, the position of the 2-(pyridin-3-yl)methyl group in compound **7a** strikingly allows it to accept a hydrogen bond from the backbone amide NH of Leu-118 in the complementary side of the receptor (Figure 6). This observation explains the structural basis of our hypothesis that introducing the 2-(pyridin-3-yl)methyl group could increase binding affinity, provided that other key interactions involving the other parts of the ligand are not significantly perturbed.

Jeffrey has classified hydrogen-bonding strength by their donor−acceptor distance D (strong if D between 2.2 and 2.5 Å; moderate if D between 2.5 and 3.2 Å; weak if D between 3.2 and 4.0 Å).[40] Applying this classification to our results shown in Table 8, we suggest that the binding affinity and selectivity of compound **7a** is dictated by the ability of the cationic center to make a moderate or strong hydrogen bond with the conserved Trp, in addition to the strong van der Waals and Coulombic interactions made between the whole ligand and the conserved Trp residue. It is noteworthy mentioning that Dougherty and co-workers have experimentally observed a cation−π interaction between serotonin and Trp-183 of the ion channel 5HT$_{3A}$ receptor.[41] Furthermore, they have demonstrated that

the high affinity of the α4β2 nAChR for nicotine results from a strong cation−π interaction between this ligand and the highly conserved Trp-149 of the principal face.[42] In addition, a hydrogen bond between the cationic center of nicotine and backbone carbonyl of that Trp is enhanced in the α4β2 nAChR. By contrast, they showed that these two key interactions are missing in the recognition of nicotine by the muscle receptor, explaining the low affinity observed in this case. That our computational results showing that the selectivity of compound **7a** for α7 nAChR vs its serotonergic 5HT$_{3A}$ homologue can be rationalized in terms of strong per residue van der Waals and Coulombic interaction and hydrogen bonding involving the cationic center and the carbonyl group of the conserved Trp, is consistent with these experimental findings. These results can be used in a docking-based virtual screening exercise aimed at predicting the binding affinity and selectivity of newly designed chemical libraries prior to their synthesis and in an external database search prior to selecting the hits to purchase. We have thus shown that in addition to cation−π interactions, these conserved Trp residues of the aromatic box strongly contribute to other noncovalent energetic interactions such as van der Walls and Coulombic interactions capable of tipping the scales of selectivity.

CONCLUSION

A novel series of 2-pyridylmethylquinuclidine carboxamides were synthesized and evaluated for their α7 nAChR selectivity. For this purpose, asymmetric synthesis of 2-pyridylmethylqui-nuclidine carboxamides (containing two stereogenic centers) was developed. A preliminary analysis of structure−activity relationships studies revealed the importance of pyridin-3-ylmethyl in position 2 of the quinuclidine ring system for enhancement of α7 nAChR affinity and α7 nAChR selectivity, especially over the 5-HT$_3$R. Comparative modeling and docking studies suggested that the selectivity of **7a** could be rationalized in terms of its interaction energy with the highly conserved Trp residue located at the binding site of nAChR and 5-HT$_3$R. The highly potent and selective α7 nAChR agonist (2S,3R)-N-[2-(pyridin-3-ylmethyl)-1-azabicyclo[2.2.2]-oct-3-yl]benzo[b]furan-2-carboxamide **7a** was identified as a promising drug candidate for the treatment of cognitive impairment associated with neurological disorders and is currently in phase 2b clinical trials as augmentation therapy to improve negative symptoms and cognition in outpatients with schizophrenia.

EXPERIMENTAL SECTION

General. All reagents and solvents were purchased from commercial vendors and were used without further purification. Reactions were monitored by thin-layer chromatography (TLC) using plates precoated with silica gel 60 F-254 (Merck) and by LCMS on Waters instrument. Flash chromatography was performed using prepacked columns supplied by Analogix and Isco. Proton (^{1}H) and carbon (^{13}C) nuclear magnetic resonance (NMR) spectra were recorded at 400 MHz on a Varian 400 spectrometer in the solvent indicated, and chemical shifts are listed in parts per million (ppm, δ) downfield of internal tetramethylsilane (δ 0.0). Final compounds were purified by preparative HPLC Gilson chromatograph using Phenomenex Gemini C18 columns (mobile phase: water−acetonitrile gradient containing 0.05% of trifluoroacetic acid) and providing purity ≥95%. Chiral separation was performed using preparative column 25 cm × 2.1 cm Chiralpak (Chiral Technologies, Inc.), eluting with hexanes−ethanol−di-n-butylamine (60:40:0.2) (flow rate 30 mL/min), and was monitored at 270 nm. Chiral HPLC analysis was performed using

analytical column Chiralpak AD (250 mm × 4.6 mm, 5 μm): mobile phase, hexanes−ethanol−di-n-butylamine (60:40:0.2); injection volume, 10 μL; flow rate, 1.0 mL per min; temperature, 20 °C; detection, UV at 270 nm; total run time, 25 min; elution order (RT), **7a** (5.3 min), **7b** (7.3 min), **7c** (8.3 min), **7d** (12.1 min). Optical rotation was measured at Autopol III automatic polarimeter (Rudolph Research Analytical). Elemental analyses were performed by Atlantic Microlab, Inc. (Norcross, Georgia). Compounds for biological testing were prepared as water-soluble pharmaceutically relevant salts. Biological spectra analysis was accomplished according to the described procedure.[43] Hierarchical clustering was carried out using the Unweighted Pair Group Method[43] with Arithmetic Mean (UPGMA), also known as average linkage method, as implemented within Spotfire DecisionSite 9.1.1. (Spotfire, Somerville, MA). Cosine correlation was used as similarity measure.

2-(Pyridin-3-ylmethylene)-1-azabicyclo[2.2.2]octan-3-one (2). Quinuclidin-3-one hydrochloride (8.25 kg, 51.0 mol) and methanol (49.5 L) were added to a 100 L glass reaction flask, under a nitrogen atmosphere, equipped with a mechanical stirrer, temperature probe, and condenser. Potassium hydroxide (5.55 kg, 99.0 mol) was added via a powder funnel over an approximately 30 min period, resulting in a rise in reaction temperature from 50 to 56 °C. Over an approximately 2 h period, pyridine-3-carboxaldehyde (4.80 kg, 44.9 mol) was added to the reaction mixture. The resulting mixture was stirred at 20 °C ± 5 °C for a minimum of 12 h, as the reaction was monitored by TLC. Upon completion of the reaction, the reaction mixture was filtered through a sintered glass funnel and the filter cake was washed with methanol (74.2 L). The filtrate was concentrated, transferred to a reaction flask, and water (66.0 L) was added. The suspension was stirred for a minimum of 30 min, filtered, and the filter cake was washed with water (90.0 L) until the pH of the rinse was 7−9. The solid was dried under vacuum at 50 °C ± 5 °C for a minimum of 12 h to provide the title compound (8.58 kg, 89.3% yield). ^{1}H NMR (CDCl₃) δ 9.07 (s, 1H), 8.56 (m, 2H), 7.34 (m, 1H), 7.00 (m, 1H), 3.19 (m, 2H), 3.00 (m, 2H), 2.67 (m, 1H), 2.08 (m, 4H). ^{13}C NMR (CD₃OD) δ 206.5, 152.7, 149.8, 148.0, 140.4, 131.9, 124.8, 121.6, 48.6, 41.4, 26.3.

(2S)-2-(Pyridin-3-ylmethyl)-1-azabicyclo[2.2.2]octan-3-one Di-p-toluoyl-D-tartrate (4). Compound **2** (5.40 kg, 25.2 mol) and methanol (40.5 L) were added to a 72 L reaction vessel under an inert atmosphere equipped with a mechanical stirrer, temperature probe, low-pressure gas regulator system, and pressure gauge. The headspace was filled with nitrogen, and the mixture was stirred to obtain a clear yellow solution. To the flask was added 10% palladium on carbon (50% wet) (270 g). The atmosphere of the reactor was evacuated using a vacuum pump, and the headspace was replaced with hydrogen to 10−20 in. water pressure. The evacuation and pressurization with hydrogen were repeated two more times, leaving the reactor under 20 in. water pressure of hydrogen gas after the third pressurization. The reaction mixture was stirred at 20 °C ± 5 °C for a minimum of 12 h, and the reaction was monitored via TLC. Upon completion of the reaction, the suspension was filtered through a bed of Celite 545 (1.9 kg) on a sintered glass funnel, and the filter cake was washed with methanol (10.1 L). The filtrate was concentrated to obtain compound **3** as a semisolid, which was transferred, under a nitrogen atmosphere, to a 200 L reaction flask fitted with a mechanical stirrer, condenser, and temperature probe. The semisolid was dissolved in ethanol (57.2 L), and di-p-toluoyl-D-tartaric acid (DTTA) (9.74 kg, 25.2 mol) was added. The stirring reaction mixture was heated at reflux for a minimum of 1 h and for an additional minimum of 12 h while the reaction was cooled to between 15 and 30 °C. The suspension was filtered using a tabletop filter, and the filter cake was washed with ethanol (11.4 L). The product was dried under vacuum at ambient temperature to obtain the title compound (11.6 kg, 76.2% yield, 59.5% factored for purity). ^{1}H NMR (free base, CDCl₃) δ 8.57 (m, 2H), 7.60 (d, 1H), 7.12 (m, 1H), 3.38 (m, 1H), 3.18 (m, 3H), 2.85 (m, 3H), 2.49 (m, 1H), 2.01 (m, 4H). ^{13}C NMR (free base, CD₃OD) δ 222.1, 151.9, 149.2, 140.1, 138.2, 126.4, 72.8, 43.2, 42.5, 33.1, 28.5, 26.6. [α]$_D^{20}$ −85.1° (c = 10 mg/mL, methanol).

(2S,3R)-3-Amino-2-(pyridin-3-ylmethyl)-1-azabicyclo[2.2.2]-octane (6a) Di-p-toluoyl-D-tartrate. Water (46.25 L) and sodium bicarbonate (4.35 kg, 51.8 mol) were added to a 200 L flask. Upon complete dissolution, dichloromethane (69.4 L) was added. Compound **4** (11.56 kg, 19.19 mol) was added, and the reaction mixture was stirred for 2−10 min. The layers were allowed to separate for a minimum of 2 min (additional water (20 L) was added when necessary to partition the layers). The organic phase was removed and dried over anhydrous sodium sulfate. Dichloromethane (34.7 L) was added to the remaining aqueous phase, and the suspension was stirred for 2−10 min. The layers were allowed to separate for between 2−10 min. Again, the organic phase was removed and dried over anhydrous sodium sulfate. The extraction of the aqueous phase with dichloromethane (34.7 L) was repeated one more time, as above. Samples of each extraction were submitted for chiral HPLC analysis. Sodium sulfate was removed by filtration, and the filtrates were concentrated to obtain (2S)-2-(pyridin-3-ylmethyl)-1-azabicyclo[2.2.2]octan-3-one (4.0 kg) as a solid. The latter (3.8 kg) was transferred to a clean 100 L glass reaction flask, under a nitrogen atmosphere, fitted with a mechanical stirrer and temperature probe. Anhydrous tetrahydrofuran (7.24 L) and (+)-(R)-α-methylbenzylamine (2.55 L, 20.1 mol) were added. Titanium(IV) isopropoxide (6.47 L, 21.8 mol) was added to the stirred reaction mixture over a 1 h period. The reaction was stirred under a nitrogen atmosphere for a minimum of 12 h. Ethanol (36.17 L) was added to the reaction mixture. The reaction mixture was cooled to below −5 °C, and sodium borohydride (1.53 kg, 40.5 mol) was added in portions, keeping the reaction temperature below 15 °C (this addition took several hours). The reaction mixture was then stirred at 15 ± 10 °C for a minimum of 1 h. The reaction was monitored by HPLC (as indicated by less than 0.5% of (2S)-2-(pyridin-3-ylmethyl)-1-azabicyclo[2.2.2]octan-3-one remaining), 2 M sodium hydroxide (15.99 L) was added and the mixture was stirred for a minimum of 10 min. The reaction mixture was filtered through a bed of Celite 545 in a tabletop funnel. The filter cake was washed with ethanol (15.23 L), and the filtrate was concentrated to obtain an oil. The concentrate was transferred to a clean 100 L glass reaction flask equipped with a mechanical stirrer and temperature probe under an inert atmosphere. Water (1 L) was added, and the mixture was cooled to 0 ± 5 °C. Then 2 M Hydrochloric acid (24 L) was added to the mixture to adjust the pH of the mixture to pH 1. The mixture was then stirred for a minimum of 10 min, and 2 M sodium hydroxide (24 L) was slowly added to adjust the pH of the mixture to pH 14. The mixture was stirred for a minimum of 10 min, and the aqueous phase was extracted with dichloromethane (3 × 15.23 L). The organic phases were dried over anhydrous sodium sulfate (2.0 kg), filtered, and concentrated to give compound **5** (4.80 kg, 84.7% yield), which was transferred to a 22 L glass flask equipped with a mechanical stirrer and temperature probe under an inert atmosphere. Water (4.8 L) was added, and the stirring mixture was cooled to 5 ± 5 °C. Concentrated hydrochloric acid (2.97 L) was slowly added to the reaction flask, keeping the temperature of the mixture below 25 °C. The resulting solution was transferred to a 72 L reaction flask containing ethanol (18 L) equipped with a mechanical stirrer, temperature probe, and condenser under an inert atmosphere. To the flask was added 10% palladium on carbon (50% wet) (311.1 g) and cyclohexene (14.36 L). The reaction mixture was heated at near-reflux for a minimum of 12 h, and the reaction was monitored by TLC. Upon completion of the reaction, the reaction mixture was cooled to below 45 °C, and it was filtered through a bed of Celite 545 (1.2 kg) on a sintered glass funnel. The filter cake was rinsed with ethanol (3 L), and the filtrate was concentrated to obtain an aqueous phase. Water (500 mL) was added to the concentrated filtrate, and this combined aqueous layer was washed with methyl tert-butyl ether (MTBE) (2 × 4.79 L). Then 2 M sodium hydroxide (19.5 L) was added to the aqueous phase to adjust the pH of the mixture to pH 14. The mixture was then stirred for a minimum of 10 min. The aqueous phase was extracted with chloroform (4 × 11.96 L), and the combined organic phases were dried over anhydrous sodium sulfate (2.34 kg). The filtrate was filtered and concentrated to obtain (2S,3R)-3-amino-2-(pyridin-3-ylmethyl)-1-azabicyclo[2.2.2]octane (3.49 kg) as oil. The

latter was transferred to a clean 100 L reaction flask equipped with a mechanical stirrer, condenser, and temperature probe under an inert atmosphere. Ethanol (38.4 L) and di-p-toluoyl-D-tartaric acid (3.58 kg, 9.27 mol) were added. The reaction mixture was heated at gentle reflux for a minimum of 1 h. The reaction mixture was then stirred for a minimum of 12 h while it was cooled to between 15 and 30 °C. The resulting suspension was filtered, and the filter cake was washed with ethanol (5.76 L). The filter cake was transferred to a clean 100 L glass reaction flask equipped with a mechanical stirrer, temperature probe, and condenser under an inert atmosphere. A 9:1 ethanol/water solution (30.7 L) was added, and the resulting slurry was heated at gentle reflux for a minimum of 1 h. The reaction mixture was then stirred for a minimum of 12 h while cooling to between 15 and 30 °C. The mixture was filtered, and the filter cake was washed with ethanol (5.76 L). The product was collected and dried under vacuum at 50 ± 5 °C for a minimum of 12 h to give the title compound (5.63 kg, 58.1% yield). The enantiomeric purity of **6a** as a free base was determined by conversion of a portion into its N-($tert$-butoxycarbonyl)-L-prolinamide, which was then analyzed for diastereomeric purity (98%) using LCMS. ^{1}H NMR (hemigalactarate, D$_2$O) δ 8.39 (m, 2H), 7.80 (d, 1H), 7.38 (m, 1H), 4.12 (s, 1H), 3.94 (s, 1H), 3.28 (m, 2H), 3.05 (m, 6H), 1.87 (m, 5H). ^{13}C NMR (free base, CD$_3$OD) δ 152.1, 152.0, 149.2, 140.2, 138.7, 126.4, 70.1, 57.2, 51.7, 42.7, 37.9, 32.4, 28.7, 20.1. $[\alpha]_D^{20}$ +76.1° (c = 10 mg/mL, water).

(2S,3R)-N-[2-(Pyridin-3-ylmethyl)-1-azabicyclo[2.2.2]oct-3-yl]benzo[b]furan-2-carboxamide (7a) p-**Toluenesulfonate.** Compound **6a** di-p-toluoyl-D-tartrate (3.64 kg, 5.96 mol) and 10% aqueous sodium chloride solution (14.4 L, 46.4 mol) were added to a 72 L glass reaction flask equipped with a mechanical stirrer under an inert atmosphere. Then 5 M sodium hydroxide (5.09 L) was added to the stirring mixture to adjust the pH of the mixture to pH 14. The mixture was then stirred for a minimum of 10 min. The aqueous solution was extracted with chloroform (4 × 12.0 L), and the combined organic layers were dried over anhydrous sodium sulfate (1.72 kg). The combined organic layers were filtered, and the filtrate was concentrated to obtain **6a** free base (1.27 kg) as oil. The latter was transferred to a 50 L glass reaction flask equipped with a mechanical stirrer under an inert atmosphere. Dichloromethane (16.5 L), triethylamine (847 mL, 6.08 mol), benzofuran-2-carboxylic acid (948 g, 5.85 mol), and O-(benzotriazol-1-yl)-N,N,N',N'-tetramethyluronium hexafluorophosphate (HBTU) (2.17 kg, 5.85 mol) were added to the reaction mixture. The mixture was stirred for a minimum of 4 h at ambient temperature, and the reaction was monitored by HPLC. Upon completion of the reaction, 10% aqueous potassium carbonate (12.7 L, 17.1 mol) was added to the reaction mixture and the mixture was stirred for a minimum of 5 min. The layers were separated, and the organic phase was washed with 10% brine (12.7 L). The layers were separated, and the organic phase was cooled to 15 ± 10 °C. Then 3 M hydrochloric acid (8.0 L) was slowly added to the reaction mixture to adjust the pH of the mixture to 1. The mixture was then stirred for a minimum of 5 min, and the layers were allowed to partition for a minimum of 5 min. The solids were filtered using a table top filter. The layers of the filtrate were separated, and the aqueous phase and the solids from the funnel were transferred to the reaction flask. Then 3 M sodium hydroxide (9.0 L) was slowly added to the flask in portions to adjust the pH of the mixture to 14. The aqueous phase was extracted with dichloromethane (2 × 16.5 L). The combined organic phases were dried over anhydrous sodium sulfate (1.71 kg). The mixture was filtered, and the filtrate was concentrated to give (2S,3R)-N-[2-(pyridin-3-ylmethyl)-1-azabicyclo[2.2.2]oct-3-y]-benzofuran-2-carboxamide (1.63 kg, 77.0% yield) as a yellow solid. (2S,3R)-N-[2-(Pyridin-3-ylmethyl)-1-azabicyclo[2.2.2]oct-3-y]-benzofuran-2-carboxamide (1.62 kg, 4.48 mol) and dichloromethane (8.60 kg) were added into a carboy. The weight/weight percent of the material in solution was determined through HPLC analysis. The solution was concentrated to an oil, acetone (4 L) was added, and the mixture was concentrated to an oily solid. Additional acetone (12 L) was added to the oily solid in the rotary evaporator bulb, and the resulting slurry was transferred to a 50 L glass reaction flask with a mechanical stirrer, condenser, temperature probe, and condenser

under an inert atmosphere. The reaction mixture was heated to 50 ± 5 °C. Water (80.7 g) was added to the solution, and it was stirred for a minimum of 10 min. p-Toluenesulfonic acid (853 g, 4.44 mol) was added to the reaction mixture in portions over approximately 15 min. The reaction mixture was heated to reflux and held at that temperature for a minimum of 30 min to obtain a solution. The reaction was cooled to 40 ± 5 °C over approximately 2 h. Isopropyl acetate (14.1 L) was added over approximately 1.5 h. The reaction mixture was slowly cooled to ambient temperature over a minimum of 10 h. The mixture was filtered, and the filter cake was washed with isopropyl acetate (3.5 L). The isolated product was dried under vacuum at 105 ± 5 °C for between 2 and 9 h to give 2.19 kg (88.5% yield) of the title product; mp 226−228 °C; $[\alpha]_D^{20}$ −13.1° (c = 10 mg/mL, methanol). ^{1}H NMR (D$_2$O) δ 8.29 (s, 1H), 7.78 (m, J = 5.1, 1H), 7.63 (d, J = 7.9, 1H), 7.54 (d, J = 7.8, 1H), 7.49 (d, J = 8.1, 2H), 7.37 (m, J = 8.3, 1H), 7.33 (m, J = 8.3, 6.9, 1.0, 1H), 7.18 (m, J = 7.8, 6.9, 1.0, 1H), 7.14 (d, J = 8.1, 2H), 7.09 (s, 1H), 6.99 (dd, J = 7.9, 5.1, 1H), 4.05 (m, J = 7.7, 1H), 3.74 (m, 1H), 3.47 (m, 2H), 3.28 (m, 1H), 3.22 (m, 1H), 3.15 (dd, J = 13.2, 4.7, 1H), 3.02 (dd, J = 13.2, 11.5, 1H), 2.19 (s, 3H), 2.02 (m, 2H), 1.93 (m, 2H), 1.79 (m, 1H). ^{13}C NMR (D$_2$O) δ 161.8, 157.2, 154.1, 150.1, 148.2, 146.4, 145.2, 138.0, 137.0, 130.9, 128.2 (2), 126.9, 126.8, 125.5 (2), 123.7, 123.3, 122.7, 111.7, 100.7, 61.3, 50.2, 48.0, 40.9, 33.1, 26.9, 21.5, 20.8, 17.0.

A sample of compound **7a** p-toluenesulphonate was converted into a free base by treatment with aqueous sodium hydroxide and extraction with chloroform. Thorough evaporation of the chloroform left an off-white powder; mp 167−170 °C; $[\alpha]_D^{20}$ −14.8° (c = 10 mg/mL, methanol) with the following spectral characteristics: positive ion electrospray MS [M + H]$^+$ ion m/z = 362. ^{1}H NMR (DMSO-d_6) δ 8.53 (d, J = 7.6 Hz, 1H), 8.43 (d, J = 1.7 Hz, 1H), 8.28 (dd, J = 1.6, 4.7 Hz, 1H), 7.77 (d, J = 7.7 Hz, 1H), 7.66 (d, J = 8.5 Hz, 1H), 7.63 (dt, J = 1.7, 7.7 Hz, 1H), 7.52 (s, 1H), 7.46 (m, J = 8.5, 7.5 Hz, 1H), 7.33 (m, J = 7.7, 7.5 Hz, 1H), 7.21 (dd, J = 4.7, 7.7 Hz, 1H), 3.71 (m, J = 7.6 Hz, 1H), 3.11 (m, 1H), 3.02 (m, 1H), 2.80 (m, 2H), 2.69 (m, 2H), 2.55 (m, 1H), 1.80 (m, 1H), 1.77 (m, 1H), 1.62 (m, 1H), 1.56 (m, 1H), 1.26 (m, 1H). ^{13}C NMR (126 MHz, DMSO-d_6) δ 158.1, 154.1, 150.1, 149.1, 146.8, 136.4, 135.4, 127.1, 126.7, 123.6, 122.9, 122.6, 111.8, 109.3, 61.9, 53.4, 49.9, 40.3, 35.0, 28.1, 26.1, 19.6.

(2S,3R)-N-[2-(Pyridin-3-ylmethyl)-1-azabicyclo[2.2.2]oct-3-yl]benzo[b]furan-2-carboxamide (7a) Hydrochloride. A hydrochloric acid/THF solution was prepared by addition of concentrated hydrochloric acid (1.93 mL of 12M, 23.2 mmol) dropwise to 8.5 mL of chilled THF. The solution was warmed to ambient temperature. To a round-bottom flask was added **7a** free base (8.49 g, 23.5 mmol) and acetone (85 mL). The mixture was stirred and heated at 45−50 °C until a complete solution was obtained. The hydrochloric acid/THF solution prepared above was added dropwise over a 5 min period, with additional THF (1.5 mL) used in the transfer. Granular, white solids began to form during the addition of the acid solution. The mixture was cooled to ambient temperature and stirred overnight (16 h). The solids were collected by suction filtration, the filter cake was washed with acetone (10 mL), and the solid was air-dried with suction for 30 min. The solid was further dried in a vacuum oven at 75 °C for 2 h to give 8.79 g of the fine white crystals (94%); mp 255−262 °C; chiral purity 98.8% (270 nm); $[\alpha]_D^{20}$ −13.8° (c = 10 mg/mL, methanol). ^{1}H NMR (300 MHz, DMSO-d_6) δ 10.7 (broad s, 1H−quaternary ammonium), 8.80 (broad s, 1H−amide H), 8.54 (s, 1H), 8.23 (d, 1H), 7.78 (d, 1H), 7.74 (d, 1H), 7.60 (d, 1H), 7.47 (m, 2H), 7.33 (m, 1H), 7.19 (m, 1H), 4.19 (m, 1H), 4.08 (m, 1H), 3.05−3.55 (m, 6H), 2.00−2.10 (m, 3H), 1.90 (m, 1H), 1.70 (m, 1H).

(2R,3S)-N-[2-(Pyridin-3-ylmethyl)-1-azabicyclo[2.2.2]oct-3-yl]benzo[b]furan-2-carboxamide (7b). To a stirred solution of **3** (3.00 g, 13.9 mmol) in dry methanol (20 mL), under nitrogen, was added a 1 M solution of zinc chloride in ether (2.78 mL, 2.78 mmol). After stirring at ambient temperature for 30 min, this mixture was treated with solid ammonium formate (10.4 g, 167 mmol). After stirring another hour at ambient temperature, solid sodium cyanoborohydride (1.75 g, 27.8 mmol) was added in portions. The reaction was then stirred at ambient temperature overnight and terminated by addition of water (5 mL). The quenched reaction was

partitioned between 5 M sodium hydroxide (10 mL) and chloroform (20 mL). The aqueous layer was extracted with chloroform (20 mL), and combined organic layers were dried over sodium sulfate, filtered, and concentrated to yield 2.97 g of crude 3-amino-2-(pyridin-3-ylmethyl)-1-azabicyclo[2.2.2]octane (**6**) as a mixture of cis- and trans-diastereomers. Di-*p*-toluoyl-D-tartaric acid (5.33 g, 13.8 mmol) was added to a stirred solution of crude **6** (6.00 g, 27.6 mmol) in methanol (20 mL). After complete dissolution, the clear solution was then concentrated to a solid mass by rotary evaporation. The solid was dissolved in a minimum amount of boiling methanol (∼5 mL). The solution was cooled slowly, first to ambient temperature (1 h), then for ∼4 h at 5 °C, and finally at −5 °C overnight. The precipitated salt was collected by suction filtration and recrystallized from 5 mL of methanol. Obtained white solid (1.4 g) was partitioned between chloroform (5 mL) and 2 M sodium hydroxide (5 mL). The chloroform layer, and a 5 mL chloroform extract of the aqueous layer were combined, dried on anhydrous sodium sulfate, and concentrated to give **6a** as colorless oil (0.434 g). The mother liquor from the initial crystallization was made basic to pH 11 with 2 M sodium hydroxide and extracted twice with chloroform (10 mL). The chloroform extracts were dried over anhydrous sodium sulfate and concentrated to give oil (3.00 g), which was dissolved in methanol (10 mL) and treated with di-*p*-toluoyl-L-tartaric acid (2.76 g, 6.90 mmol). The mixture was warmed to aid dissolution and then cooled slowly to −5 °C, where it remained overnight. The precipitate was collected by suction filtration, recrystallized from methanol, and dried to yield white solid (1.05 g). The salt was converted into the free base **6b** (0.364 g), and its enantiomeric purity (97%) was assessed by conversion of a portion into its *N*-(*tert*-butoxycarbonyl)-L-prolinamide, which was then analyzed for diastereomeric purity using LCMS. Diphenylchlorophosphate (96 μL, 124 mg, 0.46 mmol) was added dropwise to a solution of benzo[*b*]furan-2-carboxylic acid (75 mg, 0.46 mmol) and triethylamine (64 μL, 46 mg, 0.46 mmol) in dry dichloromethane (1 mL). After stirring at ambient temperature for 45 min, a solution of **6a** (0.10 g, 0.46 mmol) (that derived from the di-*p*-toluoyl-L-tartaric acid salt) and triethylamine (64 μL, 46 mg, 0.46 mmol) in dry dichloromethane (1 mL) was added. The reaction mixture was stirred overnight at ambient temperature and then treated with 10% sodium hydroxide (1 mL). The biphasic mixture was separated, and the organic layer and a chloroform extract (2 mL) of the aqueous layer were concentrated by rotary evaporation. The residue was dissolved in methanol and purified by preparative HPLC. Concentration of selected fractions, partitioning of the resulting residue between chloroform and saturated aqueous sodium bicarbonate, and evaporation of the chloroform gave 82.5 mg (50%) of **7b** as a white powder. The NMR spectrum was identical to that obtained for **7a**. $[\alpha]_D^{20}$ +12.1 (*c* = 10 mg/mL, methanol).

(2*R*,3*R*)-*N*-[2-(Pyridin-3-ylmethyl)-1-azabicyclo[2.2.2]oct-3-yl]benzo[*b*]furan-2-carboxamide (7c) and (2*S*,3*S*)-*N*-[2-(Pyridin-3-ylmethyl)-1-azabicyclo[2.2.2]oct-3-yl]benzo[*b*]furan-2-carboxamide (7d). A sample of the supernatant from the isolation of **7a** *p*-toluenesulfonate was concentrated by rotary evaporation, adjusted to pH 10 with 10% aqueous sodium hydroxide, and extracted with dichloromethane. The dichloromethane extract was evaporated, and the residue (1.8 g) was dissolved in absolute ethanol (55 mL) containing 0.5% di-*n*-butylamine. This solution was injected, in 0.25 mL portions, onto a 25 cm × 2.1 cm Chiralpak AD chiral HPLC column, eluting with hexane−ethanol−di-*n*-butylamine (60:40:0.2, flow rate = 30 mL/min), monitored at 270 nm. Isolation of the effluent eluting at 7.5 min and that eluting at 13.5 min gave, after evaporation of the solvent, **7c** (0.48 g, 98% chiral purity), $[\alpha]_D^{20}$ −62.7° (*c* = 4.7 mg/mL, methanol, and **7d** (0.47 g, 99% chiral purity), $[\alpha]_D^{20}$ +103.8° (*c* = 8 mg/mL, methanol), respectively, of colorless oil. The two NMR spectra were identical. ¹H NMR (300 MHz, CDCl₃) δ 8.49 (s, 1H), 8.45 (d, 1H), 7.74 (d, 1H), 7.52 (m, 4H), 7.35 (t, 1H), 7.20 (dd, 1H), 7.05 (d, 1H), 4.55 (dt, 1H), 3.43 (m, 1H), 3.22 (m, 1H), 2.90 (m, 5H), 2.09 (m, 1H), 1.88 (m, 4H). A warm solution of each of the free base samples **7c** and **7d** in absolute ethanol (10 mL) was treated with 1 equiv of galactaric acid. The resulting mixtures were heated at 75 °C for 5 min and cooled, with stirring, to ambient

temperature. The resulting solids were collected by suction filtration and vacuum-dried, giving 0.65 g (87%) and 0.62 g (85%), respectively, of white granular solid (mp 200−205 °C in each case). ¹H NMR (300 MHz, D₂O) δ 8.38 (s, 1H), 8.28 (d, 1H), 7.94 (d, 1H), 7.70 (d, 1H), 7.59 (d, 1H), 7.48 (t, 1H), 7.40 (m, 1H), 7.32 (m, 2H), 4.42 (m, 1H), 4.21 (s, 2H), 3.87 (s, 2H), 3.68 (m, 1H), 3.35 (m, 6H), 2.25 (m, 2H), 2.02 (m, 3H). ¹³C NMR (D₂O) δ 162.1, 157.9, 151.8, 148.8, 139.8, 129.6, 126.4, 125.1, 114.2, 113.1, 62.2, 43.0, 33.3, 29.7, 27.8, 21.4.

Binding and Ion Flux Assays. [³H]-methyllycaconitine binding to rat α7 receptors was determined in hippocampal membranes using standard methods as described previously.[44] Binding at the other receptor subtypes was performed as described previously.[45] Binding at human α7 receptors utilized HEK/human α7/RIC3 membranes (cells obtained from Dr. J. Lindstrom, Philadelphia, PA) and [³H]-epibatidine. To examine binding to α4β2 receptors, [³H]-nicotine binding to rat cortical membrane preparations or SH-EP1 human α4β2 cells (Dr. R. Lucas, Phoenix, AZ) membranes were utilized. The IC₅₀ (concentration of the compound that produces 50% inhibition of binding) was determined by least-squares nonlinear regression using GraphPad Prism software (GraphPad, San Diego, CA). The clonal cell lines PC12 (Shooter) and SH-SYSY were utilized to examine rat and human ganglion-type nicotinic receptors, respectively, and the TE671/RD clonal line was used to examine human muscle-type nicotinic receptors. Functional activation of these receptors was determined by ⁸⁶Rb⁺ efflux assays according to published protocols.[46] Receptor selectivity testing was performed by Caliper Life Sciences (formerly NovaScreen) using a customized side effects profile screen that included 65 receptor and enzyme targets.

Patch Clamp Electrophysiology. The standard external solution contained: 120 mM NaCl, 3 mM KCl, 2 mM MgCl₂, 2 mM CaCl₂, 25 mM D-glucose, and 10 mM HEPES and was adjusted to pH 7.4 with Tris base. Internal solution (pH 7.3) for whole-cell recordings consisted of 110 mM Tris phosphate dibasic, 28 mM Tris base, 11 mM EGTA, 2 mM MgCl₂, 0.1 mM CaCl₂, and 4 mM Mg-ATP. To initiate whole-cell current responses, compounds were delivered by moving cells from the control solution to agonist-containing solution and back so that solution exchange occurred within ∼50 ms (based on 10−90% peak current rise times). Intervals between compound applications (0.5−1 min) were adjusted specifically to ensure the stability of receptor responsiveness (without functional rundown), and the selection of pipet solutions used in most of the studies described here was made with the same objective. All compounds were prepared daily from stock solutions. To determine EC₅₀ values in primary screening mode, compound(s) were applied in concentrations 1 nM, 10 nM, 100 nM, 1 μM, and 10 μM). Curves were fitted with single Hill equation, and slope function was assumed to equal 1. For several advanced compounds, we ran a secondary screening test. Twelve concentrations dose response was used, and compound(s) were applied in a different concentration range (dependent upon results of primary screening) from 0.01 nM up to 1 mM. In this study, we used rat single point mutated α7 receptors stably expressed in the GH4C1 cell line.[47] After removal from the incubator, the medium was aspirated and cells were trypsinized for 3 min, washed thoroughly twice with recording medium, and resuspended in 2 mL of external solution (see below for composition). Cells were gently triturated to detach them from the plate and transferred into 4 mL test tubes from which cells were placed in the Dynaflow chip mount on the stage of an inverted Zeiss microscope (Carl Zeiss Inc., Thornwood, NY). On average, 5 min was necessary before the whole-cell recording configuration was established. To avoid modification of the cell conditions, a single cell was recorded per single load. To evoke short responses, agonists were applied for 0.5 s using a Dynaflow system (Cellectricon, Inc., Gaithersburg, MD), where each channel delivered pressure-driven solutions at either 50 or 150 psi. Conventional whole-cell current recordings was used. Glass microelectrodes (5−10 MΩ resistance) were used to form tight seals (>1 GΩ) on the cell surface until suction was applied to convert to conventional whole-cell recording. The cells were then voltage-clamped at holding potentials of −60 mV, and ion currents in response to application of ligands were measured. Whole-cell currents recorded with an Axon 700A amplifier were filtered at 1

kHz and sampled at 5 kHz by an ADC board 1440 (Molecular Devices) and stored on the hard disk of a PC computer. Whole-cell access resistance was less than 20 MΩ. Data acquisition of whole-cell currents was done using a Clampex 10 (Molecular Devices, Sunnyvale, CA), and the results were plotted using Prism 5.0 (GraphPad Software Inc., San Diego, CA). The experimental data are presented as the mean ± CI (confidential interval), and comparisons of different conditions were analyzed for statistical significance using Student's t and Two-Way ANOVA tests. All experiments were performed at room temperature (22 ± 1 °C). Concentration−response profiles were fit to the Hill equation and analyzed using Prism 5.0.

hERG Assay. The Chinese hamster ovary (CHO) cells stably expressing human hERG channels were routinely grown at 37 °C under a 5% CO_2 atmosphere, in Dulbecco's Modified Eagle's Medium/Nutrient Mixture F12 (DMEM/F12) (Invitrogen, Carlsbad, CA), supplemented with 10% heat-inactivated fetal bovine serum (FBS, Invitrogen) and 0.2 mg/mL Geneticin (MediaTech, Manassas, VA). Prior to harvesting, cell culture plates were washed twice with prewarmed Dulbecco's Phosphate Buffered Saline (DPBS, Invitrogen) and incubated for 15 min at 37 °C with 3 mL of Accutase (Innovative Cell Technologies, San Diego, CA). After incubation, 10 mL of DMEM/F12 was added to the plates and the cell suspension was triturated several times with a serological pipet. Cell suspension was then transferred into a plastic 15 mL centrifuge tube and left undisturbed for at least 15 min at 37 °C. Just prior to the experiment, cell suspension was centrifuged for 2 min at 158g, the supernatant was discarded, and the pellet was resuspended in 10 mL of recording medium. After another round of centrifugation for 2 min at 158g, the supernatant was discarded and the cell pellet was finally resuspended in 0.1 mL of recording medium. Stock solutions of all test compounds were prepared in dimethylsulfoxide (DMSO) and were stored frozen. Test concentrations were prepared by dilution stock solutions in the extracellular medium composed of (mM): NaCl, 137; KCl, 4.0; $CaCl_2$, 1.8; $MgCl_2$, 1; HEPES, 10; glucose, 10; pH was adjusted to 7.4 with NaOH solution. Test concentrations were loaded into 96-well plastic plates with flat-bottomed glass inserts. All test and control solutions contained 0.3% DMSO. The intracellular solution for whole-cell recordings was composed of (mM): potassium aspartate, 130; $MgCl_2$, 5; EGTA, 5; ATP, 4; HEPES, 10; pH 7.2 adjusted with KOH solution. All recordings were performed at ambient temperature (22 ± 3 °C) using PatchXpress 7000A automated parallel patch-clamp system (Molecular Devices, Sunnyvale, CA). SealChip electrode arrays (manufactured by AVIVA Biosciences and distributed by Molecular Devices) were loaded and automatically prepared according to the built-in procedure. For each experiment, cell suspension was triturated four times by an on-board Carvo pipetting robot and 3 μL of cell suspension was added to each well. hERG channel currents were measured using a stimulus voltage pattern consisting of a 2 s depolarizing step to +20 mV applied from a holding potential of −80 mV, followed by a 2 s repolarizing step to −50 mV. Data analysis was performed using DataXpress 2.0 software (Molecular Devices).

Single Crystal X-ray Diffraction Analysis. Single crystals of (2S,3R)-N-[2-(pyridin-3-ylmethyl)-1-azabicyclo[2.2.2]oct-3-yl]benzo-[b]furan-2-carboxamide (**7a**) as the partially hydrated hydrochloride salt and (2R,3R)-N-[2-(pyridin-3-ylmethyl)-1-azabicyclo[2.2.2]oct-3-yl]benzo[b]furan-2-carboxamide (**7c**) as a free base were analyzed on X-ray diffractometer Bruker AXS SMART 1K CCD with Mo Kα radiation source using structure solution program Bruker-AXS SHELXTL. For hydrochloride of **7a**, the Flack parameter has been determined as 0.00(5) and 1.00(5) for the inverted structure. The absolute stereochemistry has been assigned, and the configuration at the chiral centers C10 and C14 has been determined as R and S, respectively. Single crystal of **7c** as a free base does not contain any heavy atoms, and as such it was not possible to rigorously determine the absolute stereochemistry through an analysis of the Flack parameter. The determination of the absolute structure using Bayesian statistics on Bijvoet differences[48] reveals that the probability of the absolute structure being correct as drawn is 0.997, while the probability of the absolute structure being false or a racemic twin is 0.003 and 0.239, respectively. The Flack equivalent and its uncertainty

are calculated through this program to be 0.08(27). On the basis of this determination, the absolute stereochemistry has been assigned and the configuration at the chiral centers C7 and C11 has been tentatively determined as R and R, respectively.

Molecular Modeling. *a. Homology Modeling of α7, α4β2 nAChRs, and 5HT$_{3A}$ Proteins.* The primary sequence of the human α4β2, $5HT_{3A}$, and α7 proteins were extracted from the Biology Workbench 3.2 platform.[49] Three-dimensional models of the extracellular domain of the heteropentameric (α4)3(β2)2 and homopentameric $5HT_{3A}$ and α7 were obtained using the computer software package MODELER, as implemented within Discovery Studio.[50] The 3D structure of the *Aplysia californica* acetylcholine binding protein (AChBP) in complex with epibatidine (PDB code: 2byq) was used as a template for α4β2. The 3D structure of the *Lymnaea stagnalis* AChBP in complex with nicotine (PDB code: 1uw6) was used to as a template to model $5HT_{3A}$ and α7 proteins. The derived homology models were further refined within the Maestro[51] protein preparation wizard module prior to carrying out any docking studies.

b. Ligands Docking Using Glide. Docking was carried out as previously described.[52] In a nutshell, using the protein preparation wizard module, hydrogen-bonding assignment was optimized and protein−ligand complex was energy-minimized to a root-mean-square deviation (rmsd) of 0.30 Å. Standard protonation state at physiological pH was used for all ligands, i.e., the quinuclidine nitrogen was treated as protonated. Docking of ligands into homology models was carried out using Glide 5.5.[53] The docking grid was constructed using the centroid of the bound ligand in the homology model, as copied from the cocrystal structure by MODELER, and a maximum size of 20 Å for ligands to be docked. Flexibility of the OH groups of residues at the binding site was allowed. No H-bond constraint was specified. Energy-minimized structures were first docked in standard precision (SP) mode. Ten derived best poses were subsequently docked in extra precision (XP mode). Per residue interaction energies between the ligand and the protein were calculated at the XP docking stage for residues within 12 Å of grid center. All docking runs were carried out using one of the binding sites at the interface between adjacent α4 and β2 subunit for α4β2, and a homodimeric 3D model, for α7 and $5HT_{3A}$ proteins. To confirm the binding mode of ligands into the α7 nAChR protein as predicted using an homology model, we also docked the compound directly into the crystal structure of α7−AChBP chimera, which has recently been solved by Chen and co-workers,[6b] because the latter protein sequence is closer in similarity (71%) and identity (64%) to the extracellular domain of the wild-type α7 protein.

c. Calculations of the Hydrophilic/Hydrophobic Surface Areas. Hydrophilic and hydrophobic surface areas of the binding site were calculated as previously described.[44] We have used Maestro and the homodimeric interface of the homology model derived for the extracellular domain of the human α7 nAChR protein. All residues located within a 7 Å distance to the highly conserved binding site Trp residue were included in the calculation. The hydrophilic/hydrophobic surface area around a ligand pose was specifically derived from the XP visualizer module. We also utilized Pipeline Pilot (Accelrys, Inc., San Diego) to calculate the ligand solvent-accessible surface area and its volume by means of a 3D method, using a probe radius of 1.4 Å. In addition, biochemical validation of the α7, α4β2, and 5HT3 homology models were carried out by docking of diverse chemical libraries of 2288, 3955, and 40 compounds of known binding affinity to the α7, α4β2, and 5HT3 receptor subtypes, respectively. The data sets were comprised of both proprietary and competitors compounds. The performance of the docking exercise to classify compounds with respect to their binding affinity using this homology model was evaluated by means of the area under the receiver operating characteristic (ROC) curve. The ROC accuracy obtained was 0.87, 0.85, and 0.82 for the α4β2, α7, and 5HT3 homology models, respectively. It is important to mention that ROC score of 0.50 indicates random performance, while a score of 1.00 indicates a perfect model, suggesting that with a ROC score within the range of 0.82−0.87, our homology models performed well in discriminating good binders from decoys.

Article

ASSOCIATED CONTENT

Ⓢ Supporting Information

Procedures for compounds, heat map visualization of the percent inhibition values at 10 μM ligand concentration for compound **7a** and analogues, and hydrophobicity/hydrophilicity map of the α7 nAChR protein binding site. This material is available free of charge via the Internet at http://pubs.acs.org

AUTHOR INFORMATION

Corresponding Author

*Phone: (336) 545-8010. E-mail: galana99@yahoo.com.

Notes

The authors declare no competing financial interest.

ABBREVIATIONS USED

AChBP, acetylcholine binding proteins; CHO, Chinese hamster ovary cells; EGTA, ethylene glycol tetraacetic acid; DMEM, Dulbecco's Modified Eagle's Minimal Essential Medium; FBS, fetal bovine serumHEPES, 4-(2-hydroxyethyl)-1-piperazineethanesulfonic acid; E_{max}, maximum effect achievable, efficacy; kD, kilodalton; Mg-ATP, magnesium ATPase; HBTU, *O*-(benzotriazol-1-yl)-*N*,*N*,*N'*,*N'*-tetramethyluronium hexafluorophosphate; PC-12, rat pheochromocytoma cells; SH-SYSY, hyman neuroblastoma cell line; SH-EP1, human epithelial cells; LBD, ligand binding domain; ROC, receiver operating characteristic curve; Tris, tris(hydroxymethyl)-aminomethane; PDB, protein databank; rmsd, root-mean-square deviation; SP, standard precision; XP, extra precision

REFERENCES

(1) Lippiello, P. M.; Bencherif, M.; Hauser, T. A.; Jordan, K. G.; Letchworth, S. R.; Mazurov, A. A. Nicotinic Receptors as Targets for Therapeutic Discovery. *Expert Opin. Drug Discovery* **2007**, *2* (9), 1185−1203.

(2) Law, R. J.; Henchman, R. H.; McCammon, J. A. A gating mechanism proposed from a simulation of a human α7 nicotinic acetylcholine receptor. *Proc. Natl. Acad. Sci. U. S. A.* **2005**, *102*, 6813−6818.

(3) (a) Schrattenholz, A.; Coban, T.; Schröder, B.; Okonjo, K. O.; Kuhlmann, J.; Pereira, E. F.; Albuquerque, E. X.; Maelicke, A. Biochemical Characterization of a Novel Channel-Activating Site on Nicotinic Acetylcholine Receptors. *J. Recept. Res.* **1993**, *13*, 393−412. (b) Tomizawa, M.; Maltby, D.; Medzihradszky, K. F.; Zhang, N.; Durkin, K. A.; Presley, J.; Talley, T. T.; Taylor, P.; Burlingame, A. L.; Casida, J. E. Defining Nicotinic Agonist Binding Surfaces through Photoaffinity Labeling. *Biochemistry* **2007**, *46*, 8798−8806.

(4) Brejc, K.; van Dijk, W. J.; Klaassen, R. V.; Schuurmans, M.; van Der Oost, J.; Smit, A. B.; Sixma, T. K. Crystal Structure of an ACh-Binding Protein Reveals the Ligand-Binding Domain of Nicotinic Receptors. *Nature* **2001**, *411*, 269−276.

(5) (a) Celie, P. H.; van Rossum-Fikkert, S. E.; van Dijk, W. J.; Brejc, K.; Smit, A. B.; Sixma, T. K. Nicotine and carbamylcholine Binding to Nicotinic Acetylcholine Receptors as Studied in AChBP Crystal Structures. *Neuron* **2004**, *41*, 907−914. (b) Hansen, S. B.; Talley, T. T.; Radic, Z.; Taylor, P. Structural and Ligand recognition Characteristics of an Acetylcholine-Binding Protein from *Aplysia Californica*. *J. Biol. Chem.* **2004**, *279*, 24197−24202. (c) Celie, P. H.; Klaassen, R. V.; van Rossum-Fikkert, S. E.; van Elk, R.; van Nierop, P.; Smit, A. B.; Sixma, T. K. Crystal Structure of Acetylcholine-Binding Protein from *Bulinus Truncatus* Reveals the Conserved Structural Scaffold and Sites of Variation in Nicotinic Acetylcholine Receptors. *J. Biol. Chem.* **2005**, *280*, 26457−26466. (d) Celie, P. H.; Kasheverov, I. E.; Mordvintsev, D. Y.; Hogg, R. C.; van Nierop, P.; van Elk, R.; van Rossum-Fikkert, S. E.; Zhmak, M. N.; Bertrand, D.; Tsetlin, V.; Sixma, T. K.; Smit, A. B.

Crystal Structure of Nicotinic Acetylcholine Receptor Homolog AChBP in Complex with an Alpha-Conotoxin PnIA Variant. *Nature Struct. Mol. Biol.* **2005**, *12*, 582−588. (e) Hansen, S. B.; Sulzenbacher, G.; Huxford, T.; Marchot, P.; Taylor, P.; Bourne, Y. Structures of *Aplysia* AChBP Complexes with Nicotinic Agonists and Antagonists Reveal Distinctive Binding Interfaces and Conformations. *EMBO J.* **2005**, *24*, 3635−3646. (f) Ulens, C.; Hogg, R. C.; Celie, P. H.; Bertrand, D.; Tsetlin, V.; Smit, A. B.; Sixma, T. K. Structural Determinants of Selective Alpha-Conotoxin Binding to a Nicotinic Acetylcholine Receptor Homolog AChBP. *Proc. Natl. Acad. Sci. U. S. A.* **2006**, *103*, 3615−3620. (g) Dutertre, S.; Ulens, C.; Buttner, R.; Fish, A.; van Elk, R.; Kendel, Y.; Hopping, G.; Alewood, P. F.; Schroeder, C.; Nicke, A.; Smit, A. B.; Sixma, T. K.; Lewis, R. J. AChBP-Targeted Alpha-Conotoxin Correlates Distinct Binding Orientations with nAChR Subtype Selectivity. *EMBO J.* **2007**, *26*, 3858−3867.

(6) (a) Nemecz, A.; Taylor, P. Creating an α7 Nicotinic Acetylcholine Recognition Domain from the Acetylcholine-Binding Protein: Crystallographic and Ligand Selectivity Analyses. *J. Biol. Chem.* **2011**, *286*, 4255−4265. (b) Li, S. X.; Huang, S.; Bren, N.; Noridomi, K.; Dellisanti, C. D.; Sine, S. M.; Chen, L. Ligand-Binding Domain of an α7-Nicotinic Receptor Chimera and its Complex with Agonist. *Nature Neurosci.* **2011**, *14*, 1253−1259.

(7) (a) Tasso, B.; Canu Boido, C.; Terranova, E.; Gotti, C.; Riganti, L.; Clementi, F.; Artali, R.; Bombieri, G.; Meneghetti, F.; Sparatore, F. Synthesis, Binding, and Modeling Studies of New Cytisine Derivatives, as Ligands for Neuronal Nicotinic Acetylcholine Receptor Subtypes. *J. Med. Chem.* **2009**, *52*, 4345−4357. (b) Srivastava, S.; Hamouda, A. K.; Pandhare, A.; Duddempudi, P. K.; Sanghvi, M.; Cohen, J. B.; Blanton, M. P. [³H] Epibatidine Photolabels Nonequivalent Amino Acids in the Agonist Binding Site of Torpedo and α4β2 Nicotinic Acetylcholine Receptors. *J. Biol. Chem.* **2009**, *284*, 24939−24947. (c) Bisson, W. H; Scapozza, L.; Westera, G.; Mu, L.; Schubiger, P. A. Ligand Selectivity for the Acetylcholine Binding Site of the Rat α4β2 and α3β4 Nicotinic Subtypes Investigated by Molecular Docking. *J. Med. Chem.* **2005**, *48*, 5123−5130. (d) Huang, X.; Zheng, F.; Stokes, C.; Papke, R. L.; Zhan, C.-G. Modeling Binding Modes of R7 Nicotinic Acetylcholine Receptor with Ligands: The Roles of Gln117 and Other Residues of the Receptor in Agonist Binding. *J. Med. Chem.* **2008**, *51*, 6293−6302. (e) Le Novere, N.; Grutter, T.; Changeux, J.-P. Models of the Extracellular Domain of the Nicotinic Receptors and of Agonist- and Ca²⁺-Binding Sites. *Proc. Natl. Acad. Sci. U. S. A.* **2002**, *99*, 3210−3215. (e) Huang, X.; Zheng, F.; Chen, X.; Crooks, P. A.; Dwoskin, L. P.; Zhan, C.-G. Modeling Subtype-Selective Agonists Binding with α4β2 and α7 Nicotinic Acetylcholine Receptors: Effects of Local Binding and Long-Range Electrostatic Interactions. *J. Med. Chem.* **2006**, *49*, 7661−7674. (f) Bisson, W. H.; Westera, G.; Schubiger, P. A.; Scapozza, L. Homology Modeling and Dynamics of the Extracellular Domain of Rat and Human Neuronal Nicotinic Acetylcholine Receptor Subtypes α4β2 and α7. *J. Mol. Model.* **2008**, *14*, 891−899. (g) Taly, A.; Corringer, P.-J.; Guedin, D.; Lestage, P.; Changeux, J. P. Nicotinic Receptors: Allosteric Transitions and Therapeutic Targets in the Nervous System. *Nature Rev.* **2009**, *8*, 733−750.

(8) (a) Guandalini, L.; Martini, E.; Dei, S.; Manetti, D.; Scapecchi, S.; Teodori, E.; Romanelli, M. N; Varani, K.; Greco, G.; Spadola, L.; Novellino, E. Design of Novel Nicotinic Ligands through 3D Database Searching. *Bioorg. Med. Chem.* **2005**, *13*, 799−807. (b) Nicolotti, O.; Pellegrini-Calace, M.; Carrie, A.; Altomare, C.; Centeno, N. B.; Sanz, F.; Carottia, A. Neuronal Nicotinic Receptor Agonists: a Multi-Approach Development of the Pharmacophore. *J. Comput.-Aided Mol. Des.* **2001**, *15*, 859−872. Erratum in: *J. Comput.-Aided Mol. Des.* **2001**, *15*, 1153. (c) Beers, W. H.; Reich, E. Structure and Activity of Acetylcholine. *Nature* **1970**, *228*, 917−922. (d) Sheridan, R. P.; Nilakantan, R.; Dixon, J. S.; Venkataraghavan, R. J. The Ensemble Approach to Distance Geometry: Application to the Nicotinic Pharmacophore. *J. Med. Chem.* **1986**, *29*, 899−906. (e) Nicolotti, O.; Pellegrini-Calace, M.; Carrieri, A.; Altomare, C.; Centeno, N. B.; Sanz, F.; Carotti, A. Neuronal nicotinic Receptor Agonists: a Multi-Approach Development of the Pharmacophore. *J. Comput.-Aided Mol. Des.* **2001**, *15*, 859−872.

(9) Marks, M. J.; Collins, A. C. Characterization of nicotine binding in mouse brain and comparison with the binding of alpha-bungarotoxin and quinuclidinyl benzilate. *Mol. Pharmacol.* **1982**, *3*, 554–564.

(10) Freedman, R.; Hall, M.; Adler, L. E.; Leonard, S. Evidence in Post-Mortem Brain Tissue for Decreased Numbers of Hippocampal Nicotinic Receptors in Schizophrenia. *Biol. Psychiatry* **1995**, *38*, 22–33.

(11) Bertrand, D.; Gopalakrishnan, M. Allosteric modulation of nicotinic acetylcholine receptors. *Biochem. Pharmacol.* **2007**, *74*, 1155–1163.

(12) Freedman, R.; Coon, H.; Myles-Worsley, M.; Orr-Urtreger, A.; Olincy, A.; Davis, A.; Polymeropoulos, M.; Holil, J.; Hopkins, J.; Hoff, M.; Rosenthal, J.; Waldo, M. C.; Reimherr, F.; Wender, P.; Yaw, J.; Young, D. A.; Breese, C. R.; Adams, C.; Patterson, D.; Adler, L. E.; Kruglyak, L.; Leonard, S.; Byerley, W. Linkage of a Neurophysiological Deficit in Schizophrenia to a Chromosome 15 Locus. *Proc. Natl. Acad. Sci.U. S. A.* **1997**, *94*, 587–592.

(13) Gurley, D. A.; Lanthorn, T. H. Nicotinic Agonists Competitively Antagonize Serotonin at Mouse 5HT$_3$ Receptors Expressed in *Xenopus* Oocytes. *Neurosci. Lett.* **1998**, *247*, 107–110.

(14) Karlin, A.; Akabas, M. H. Toward a structural basis for the function of nicotinic acetylcholine receptors and their cousins. *Neuron* **1995**, *15*, 1231–1244.

(15) Phillips, E.; Mack, R.; Macor, J.; Semus, S. Novel Spiroazabicyclic Heterocyclic Compounds. WO Patent 9903859, 1999.

(16) (a) Baker, S. R.; Boot, J.; Brunavs, M.; Dobson, D.; Green, R.; Hayhurst, L.; Keenan, M.; Wallace, L. High Affinity Ligands for the α7 Nicotinic Receptor that Show No Cross-Reactivity with the 5HT$_3$ Receptor. *Bioorg. Med. Chem. Lett.* **2005**, *15*, 4727–4730. (b) Macor, J. E.; Gurley, D.; Lanthorn, T.; Loch, J.; Mack, R. A.; Mullen, G.; Tran, O.; Wright, N.; Gordon, J. C. The 5-HT$_3$ Antagonist Tropisetron (ICS 205–930) is a Potent and Selective α7 Nicotinic Receptor Partial Agonist. *Bioorg. Med. Chem. Lett.* **2001**, *11*, 319–321.

(17) (a) Thompson, A. J.; Lummis, S. C. R. 5-HT$_3$ Receptors. *Curr. Pharm. Des.* **2006**, *12*, 3615–3630. (b) Cappelli, A.; Anzini, M.; Vomero, S.; Mennuni, L.; Makovec, F.; Hamon, M.; De Benedetti, P. G.; Menziani, M. C. The Interaction of 5-HT$_3$ Receptors with Arylpiperazine, Tropane, and Quinuclidine Ligands. *Curr. Top. Med. Chem* **2002**, *2*, 599–624. (c) Romanelli, M. N.; Gratteri, L.; Guandalini, L.; Martini, E.; Bonaccini, C.; Gualtieri, F. Central Nicotinic Receptors: Structure, Function, Ligands, and Therapeutic Potential. *ChemMedChem* **2007**, *2*, 2–24.

(18) (a) *Dolasetron (Anzemet) Product Information*; Aventis: Bridgewater, NJ, February 2002. (b) *Granisetron (Kytril) Product Information*; Roche: Basel, August 2002. (c) *Ondansetron (Zofran) Product Information*; GlaxoSmithKline: Research Triangle Park, NC, May 2001. (d) Lisi, D. M. Lotronex Withdrawal. *Arch. Intern. Med.* **2002**, *162*, 101.

(19) Mazurov, A. A; Speake, J. D.; Yohannes, D. Discovery and Development of α7 Nicotinic Acetylcholine Receptor Modulators. *J. Med. Chem.* **2011**, *54*, 7943–7961.

(20) Wishka, D. G.; Walker, D. P.; Yates, K. M.; Reitz, S. C.; Jia, S.; Myers, J. K.; Olson, K. I.; Jacobsen, E. J.; Wolfe, M. L.; Groppi, V. E.; Hanchar, A. J.; Thornburgh, B. A.; Cortes, B.; Luz, A.; Wong, E. H. F.; Staton, B. A.; Raub, T. J.; Higdon, N. R.; Wall, T. M.; Hurst, R. S.; Walters, R. R.; Hoffmann, W. E.; Hajos, M.; Franklin, S.; Carey, G.; Gold, L. H.; Cook, K. K.; Sands, S. B.; Zhao, S. X.; Soglia, J. R.; Kalgutkar, A. S.; Arneric, S. P.; Rogers, B. N. Discovery of *N*-[(3*R*)-1-Azabicyclo-[2.2.2]oct-3-yl]furo[2,3-*c*]pyridine-5-carboxamide, an Agonist of the α7 Nicotinic Acetylcholine Receptor, for the Potential Treatment of Cognitive Deficits in Schizophrenia: Synthesis and Structure–Activity Relationship. *J. Med. Chem.* **2006**, *49*, 4425–4436.

(21) Wall, T. M.; Hurst, R. S.; Wong, E. H. F.; Rogers, B. N. Design, Synthesis, Structure–Activity Relationship, and in Vivo Activity of Azabicyclic Aryl Amides as α7 Nicotinic Acetylcholine Receptor Agonists. *Bioorg. Med. Chem.* **2006**, *14*, 8219–8248.

(22) Malysz, J.; Anderson, D. J.; Grønlien, J. H.; Ji, J.; Bunnelle, W. H.; Håkerud, M.; Thorin-Hagene, K.; Ween, H.; Helfrich, R.; Hu, M.;

Gubbins, E.; Gopalakrishnan, S.; Puttfarcken, P. S.; Briggs, C. A.; Li, J.; Meyer, M. D.; Dyhring, T.; Ahring, P. K.; Nielsen, E. Ø.; Peters, D.; Timmermann, D. B.; Gopalakrishnan, M. In Vitro Pharmacological Characterization of a Novel Selective α7 Neuronal Nicotinic Acetylcholine Receptor Agonist ABT-107. *J. Pharm. Exp. Ther.* **2010**, *334*, 863–874.

(23) Sydserff, S.; Sutton, E. J.; Song, D.; Quirk, M. C.; Maciag, C.; Li, C.; Gerald Jonak, G.; Gurley, D.; Gordon, J. C.; Christian, E. P.; Doherty, J. J.; Hudzik, T.; Johnson, E.; Mrzljak, L.; Piser, T.; Smagin, G. N.; Wang, Y.; Widzowski, D.; Smith, J. S. Selective α7 Nicotinic Receptor Activation by AZD0328 Enhances Cortical Dopamine Release and Improves Learning and Attentional Processes. *Biochem. Pharmacol.* **2009**, *78*, 880–888.

(24) Mazurov, A.; Hauser, T.; Miller, C. H. Selective α7 Nicotinic Acetylcholine Receptor Ligands. *Curr. Med. Chem.* **2006**, *13*, 1567–1584.

(25) Langlois, M.; Meyer, C.; Soulier, J. L. Synthesis of (*R*)- and (*S*)-3-Aminoquinuclidinone from 3-Quinuclidine and (*S*)- and (*R*)-1-Phenethylamine. *Synth. Commun.* **1992**, *22*, 1895–1911.

(26) Wong, E.; Cortes-Burgos, L. A.; Rogers, B. N.; Piotrowski, D. W.; Walker, D. P.; Jacobsen, E. J.; Wishka, D. G.; Acker, B. A. Compounds Having both α7 Nicotinic Agonist Activity and 5HT3 Antagonist Activity for Treatment of CNS Diseases. WO Patent 04039815, 2004.

(27) Dwoskin, L. P.; Xu, R.; Ayers, J. T.; Crooks, P. A. Recent Developments in Neuronal Nicotinic Acetylcholine Receptor Antagonists. *Exp. Opin. Ther. Pat.* **2000**, *10*, 1561–1581.

(28) Jacobsen, E. J., Walker, D. P., Myers, J. K., Piotrowski, D. W.; Groppi, V. E. Substituted 2-Azabicyclic Moieties for the Treatment of Disease (Nicotinic Acetylcholine Receptor Antagonists). PCT WO 02/085901, 2002.

(29) Mazurov, A, A.; Klucik, J.; Miao, L.; Phillips, T. Y.; Seamans, A.; Schmitt, J. D.; Hauser, T. A.; Johnson, R. T.; Miller, C. 2-(Arylmethy)l-3-Substituted Quinuclidines as Selective α7 Nicotinic Receptor Ligands. *Bioorg. Med. Chem. Lett.* **2005**, *15*, 2073–2077.

(30) O'Donnell, C. J.; Rogers, B. N.; Bronk, B. S.; Bryce, D. K.; Coe, J. W.; Cook, K. K.; Duplantier, A. J.; Evrard, E.; Hajós, M.; Hoffmann, W. E.; Hurst, R. S.; Maklad, N.; Mather, R. J.; McLean, S.; Nedza, F. M.; O'Neill, B. T.; Peng, L.; Qian, W.; Rottas, M. M.; Sands, S. B.; Schmidt, A. W.; Shrikhande, A. V.; Spracklin, D. K.; Wong, D. F.; Zhang, A.; Zhang, L. Discovery of 4-(5-Methyloxazolo[4,5-*b*]pyridin-2-yl)-1,4-diazabicyclo[3.2.2]nonane (CP-810,123), a Novel α7 Nicotinic Acetylcholine Receptor Agonist for the Treatment of Cognitive Disorders in Schizophrenia: Synthesis, SAR Development, and in Vivo Efficacy in Cognition Models. *J. Med. Chem.* **2010**, *53*, 1222–1237.

(31) Callahan, P. M.; Wang, S.; Xie, W.; Dragan, S.; Sun, S.; Michael, T.; Herbert, B.; Rowe, W.; Tehim, A.; Lowe, D.; Barrett, J. E. Pharmacological Characterization of MEM-3454, a Novel Nicotinic Alpha7 Receptor Partial Agonist. Therapeutic Potential for the Cognitive Deficits Associated with Alzheimer's Disease and Schizophrenia. *Neuropsychopharmacology* **2006**, *31*, S198.

(32) Kalgutkar, A. S.; Gardner, I.; Obach, R. S.; Shaffer, C. I.; Callegari, E.; Henne, K.; Mutlib, A.; Dalvie, D.; Lee, J.; Nakai, Y.; O'Donell, J.; Boer, J.; Harriman, S. A. Comprehensive Listing of Bioactivation Pathways of Organic Functional Groups. *Curr. Drug Metab.* **2005**, *6*, 161–225.

(33) Deepak, K. D.; Kalgutkar, A. S.; Khojasteh-Bakht, S. C.; Obach, R. S.; O'Donell, J. P. Biotransformation Reactions of Five-Membered Aromatic Heterocyclic Rings. *Chem. Res. Toxicol.* **2002**, *15*, 269–299.

(34) Hauser, T. A.; Kucinski, A.; Jordan, K. G.; Gatto, G. J.; Wersinger, S. R.; Hesse, R. A.; Stachowiak, E. K.; Stachowiak, M. K.; Papke, R. L.; Lippiello, P. M.; Bencherif, M. TC-5619: An Alpha7 Neuronal Nicotinic Receptor-Selective Agonist that Demonstrates Efficacy in Animal Models of the Positive and Negative Symptoms and Cognitive Dysfunction of Schizophrenia. *Biochem. Pharmacol* . **2009**, *78*, 803–812.

(35) Tcheremissine, O. V.; Castro, M. A.; Dineen, R; Gardne, D. R. Targeting cognitive deficits in schizophrenia: a review of the development of a new class of medicines from the perspective of

community mental health researchers. *Exp. Opin. Invest. Drugs* **2012**, *21*, 7−14. (b) Dunbar, G.; Hosford, D.; Segreti, A.; Lieberman, J. Effects of alpha7 nicotinic receptor agonist TC-5619 in cognitive dysfunction in schizophrenia. *Eur. Neuropsychopharmacology* **2011**, *21*, S522.

(36) Prickaerts, J.; van Goethem, N. P.; Chesworth, R.; Shapiro, G.; Boess, F. G.; Methfessel, C.; Reneerkens, O. A. H.; Flood, D. G.; Hilt, D.; Gawryl, M.; Bertrand, S.; Bertrand, D.; König, G. EVP-6124, a Novel and Selective α7 Nicotinic Acetylcholine Receptor Partial Agonist, Improves Memory Performance by Potentiating the Acetylcholine Response of α7 Nicotinic Acetylcholine Receptors. *Neuropharmacology* **2012**, *62*, 1099−1110.

(37) Biton, B.; Bergis, O.; Galli, F.; Nedelec, A.; Lochead, A.; Jegham, S.; Godet, D.; Laneau, C.; Santamaria, R.; Chesney, F.; Leonardon, J.; Granger, P.; Debono, M. W.; Bohme, G. A.; Sgard, F.; Besnard, F.; Graham, D.; Coste, A.; Oblin, A.; Curet, O.; Vige, X.; Voltz, C.; Rouquie, L.; Souilhac, J.; Santucci, V.; Gueudet, C.; Francon, D.; Steinberg, R.; Griebel, G.; Oury-Donat, F.; George, P.; Avenet, P.; Scatton, B. SSR180711, a novel selective α7 nicotinic receptor partial agonist: (1) binding and functional profile. *Neuropsychopharmacology* **2007**, *32*, 1−16.

(38) Wallace, T. L.; Callahan, P. M.; Tehim, A.; Bertrand, D.; Tombaugh, G.; Wang, S.; Xie, W.; Rowe, W. B.; Ong, V.; Graham, E.; Terry, A. V., Jr.; Rodefer, J.; Herbert, B.; Murray, M.; Porter, R.; Santarelli, L.; Lowe, D. A. RG3487, a novel nicotinic α7 receptor partial agonist, improves cognition and sensorimotor gating in rodents. *J. Pharmacol. Exp. Ther.* **2011**, *336* (1), 242−253.

(39) Celie, P. H. N.; Rossum-Fikkert, S. E.; Dijk, W. J.; Brejc, K.; Smit, A. B.; Sixma, T. K. Nicotine and Carbamylcholine Binding to Nicotinic Acetylcholine Receptors as Studied in AChBP Crystal Structures. *Neuron* **2004**, *41*, 907−914.

(40) Jeffrey, G. A. *An Introduction to Hydrogen Bonding (Topics in Physical Chemistry)*; Oxford University Press: New York, 1997.

(41) Beene, D. L.; Brandt, G. S.; Zhong, W.; Zacharias, N. M.; Lester, H. A.; Dougherty, D. A. Cation−π Interactions in Ligand Recognition by Serotonergic (5-HT3A) and Nicotinic Acetylcholine Receptors: The Anomalous Binding Properties of Nicotine. *Biochemistry* **2002**, *41*, 10262−10269.

(42) Xiu, X.; Puskar, N. L.; Shanata, J. A. P.; Lester, H. A.; Dougherty, D. A. Nicotine Binding to Brain Receptors Requires a Strong Cation−π Interaction. *Nature* **2009**, *458*, 534−537.

(43) Legendre, L. *Numerical Ecology*; Elsevier: Amsterdam, 1998; pp 319−321.

(44) Davies, A. R.; Hardick, D. J.; Blagbrough, I. S.; Potter, B. V.; Wolstenholme, A. J.; Wonnacott, S. Characterization of the Binding of [³H]methyllycaconitine: A New Radioligand for Labelling of Alpha 7-Type Neuronal Nicotinic Acetylcholine Receptors. *Neuropharmacology* **1999**, *38*, 679−690.

(45) Hauser, T. A.; Hepler, C. D.; Kombo, D. C.; Grinevich, V. P.; Kiser, M. N.; Hooker, D. N.; Zhang, J.; Mountfort, D.; Selwood, A.; Akireddy, S. R.; Letchworth, S. R.; Yohannes, D. Comparison of Acetylcholine Receptor Interactions of the Marine Toxins, 13-Desmethylspirolide C and Gymnodimine. *Neuropharmacology* **2012**, *62*, 2238−2249.

(46) Bencherif, M.; Schmitt, J. D.; Bhatti, B. S.; Crooks, P.; Caldwell, W. S.; Lovette, M. E.; Fowler, K.; Reeves, L.; Lippiello, P. M. The Heterocyclic Substituted Pyridine Derivative (±)-2-(3-Pyridinyl-1)-1-azabicyclo[2.2.2]octane (RJR-2429): A Selective Ligand at Nicotinic Acetylcholine Receptors. *J. Pharmacol. Exp. Ther.* **1998**, *284*, 886−894.

(47) Placzek, A. N.; Grassi, F.; Meyer, E. M.; Papke, R. L. An α7 Nicotinic Acetylcholine Receptor Gain-of-Function Mutant That Retains Pharmacological Fidelity. *Mol. Pharmacol.* **2005**, *68*, 1863−1876.

(48) Hooft, R. W. W.; Straver, L. H.; Spek, A. L. Determination of Absolute Structure Using Bayesian Statistics on Bijvoet Differences. *J. Appl. Crystallogr.* **2008**, *41*, 96−103.

(49) *Biology Workbench 3.2*; San Diego Supercomputer Center, UCSD: San Diego, CA.

(50) (a) Eswar, N.; Marti-Renom, M. A.; Webb, B.; Madhusudhan, M. S.; Eramian, D.; Shen, M.; Pieper, U.; Sali, A. Comparative Protein Structure Modeling With MODELLER. In *Current Protocols in Bioinformatics*; John Wiley & Sons, Inc.: New York, 2006; Supplement 15, 5.6.1−5.6.30, 200. (b) Marti-Renom, M. A.; Stuart, A.; Fiser, A.; Sánchez, R.; Melo, F.; Sali, A. Comparative Protein Structure Modeling of Genes and Genomes. *Annu. Rev. Biophys. Biomol. Struct.* **2000**, *29*, 291−325. (c) *MODELER*; Accelrys, Inc: San Diego, CA, USA.

(51) *Maestro*; Schrodinger, Inc.: 101 SW Main Street, Suite 1300, Portland, OR 97204.

(52) Kombo, D. C.; Mazurov, A. A.; Tallapragada, K.; Hammond, P. S.; Chewning, J.; Hauser, T. A.; Vasquez-Valdivieso, M.; Yohannes, D.; Talley, T. T.; Taylor, P.; Caldwell, W. S. Computational Studies of Benzylidene Anabaseine Interactions with α7 Nicotinic Acetylcholine Receptor (nAChR) and Acetylcholine Binding Proteins (AChBPs): Application to the Design of Related α7 Selective Ligands. *Eur. J. Med. Chem.* **2011**, *46*, 5625−5635.

(53) (a) Friesner, R. A.; Banks, J. L.; Murphy, R. B.; Halgren, T. A.; Klicic, J. J.; Mainz, D. T.; Repasky, M. P.; Knoll, E. H.; Mee, S.; Perry, J. K.; Shaw, D. E.; Francis, P.; Shenkin, P. S. Glide: a New Approach for Rapid, Accurate Docking and Scoring. 1. Method and Assessment of Docking Accuracy. *J. Med. Chem.* **2004**, *47*, 1739−1749. (b) Halgren, T. A.; Murphy, R. B.; Friesner, R. A.; Beard, H. S.; Frye, L. L.; Pollard, W. T.; Banks, J. L. Glide: a New Approach for Rapid, Accurate Docking and Scoring. 2. Enrichment Factors in Database Screening. *J. Med. Chem.* **2004**, *47*, 1750−1759.